Exploring the relationship between relative humidity and aerosol attenuated backscatter

Geoscience & Remote Sensing

Charlotte Braat

TU Delft

Exploring the relationship between relative humidity and aerosol attenuated backscatter

Geoscience & Remote Sensing

by

Charlotte Braat

to obtain the degree of Bachelor of Science
at the Delft University of Technology,
to be defended publicly on Tuesday January 23, 2017 at 10:30 AM.

Student number: 4313488
Project duration: November 20, 2017 – January 22, 2018
Thesis committee: Prof. dr. ir. H.W.J. Russchenberg, TU Delft, supervisor
Ir. D. Mamali, TU Delft

An electronic version of this thesis is available at http://repository.tudelft.nl/.

TU Delft

Preface

I hereby present the paper 'Exploring the relationship between relative humidity and aerosol attenuated backscatter'. This paper is written as concluding report of the Bachelor Thesis for the bachelor Civil Engineering at the Delft Technical University.

The research was done at the Geoscience & Remote Sensing department of the Faculty of Civil Engineering & Geosciences at the Delft Technical University. The research subject was formulated together with my supervisors, Herman Russchenberg and Dimitra Mamali.

I would like to thank Henk Klein Baltink (KNMI) for promptly answering my questions and for processing raw lidar data for my research. I would also like to thank Stephanie Rusli, for offering her help and sharing her ideas in the startup phase of the project. Lastly, I would like to thank my supervisors for their time, effort and inspiration and their guidance throughout the thesis.

I hope you find this report enjoyable and informative.

Charlotte Braat
Delft, January 2018

Contents

List of Figures iv

1 Abstract 1

2 Introduction 2

3 Theoretical Background 3
3.1 Atmospheric aerosols . . . 3
3.1.1 Aerosol-Solar Radiation Interactions: Direct Effect . . . 4
3.1.2 Aerosol-Solar Radiation Interactions: Indirect Effect . . . 4
3.2 Hygroscopicity . . . 5
3.2.1 Measuring hygroscopicity . . . 6

4 Observations from CESAR Observatory 7
4.1 General description of the CESAR Observatory . . . 7
4.2 Instrumentation . . . 7
4.3 ACCEPT campaign . . . 7

5 Methodology 8
5.1 Data selection . . . 8
5.2 Data processing . . . 8

6 Results and Discussion 9
6.1 Lidar attenuated backscatter ratio: Case studies with variable RH . . . 9
6.1.1 15th of October . . . 9
6.1.2 25th of October . . . 12
6.1.3 10th of November . . . 15
6.2 Lidar attenuated backscatter ratio: Case studies with constant RH . . . 19
6.2.1 13th of October . . . 19
6.2.2 25th of October . . . 21
6.2.3 30th of October . . . 23
6.2.4 4th of November . . . 25
6.2.5 12th of November . . . 27

7 Conclusion and Recommendations 29

Bibliography 30

A Supervisor Meetings 33
A.1 Overview of meetings with supervisors . . . 33
A.2 Exploratory meetings with Herman Russchenberg . . . 33
A.3 ACTRIS . . . 33
A.4 Kick-off meeting with Herman Russchenberg, Dimitra Mamali and Stephanie Rusli . . . 33
A.5 Work plan meeting with Herman Russchenberg and Dimitra Mamali . . . 34
A.6 Midterm meeting with Dimitra Mamali . . . 34

List of Figures

3.1 Aerosol number concentration normalized by the width of the size range against the logarithm of the diameter for a typical example of aerosol size information [19]. . . . 3
3.2 **a.** Köhler curve, showing equilibrium relative humidities over droplets of different radius with various solutes. T = 0°C. Solute mass = 10^{-16} g. **b.** Blow-up of Figure a, highlighting the two opposing effects of evaporation and condensation [19]. . . . 5
3.3 Diameter change of $(NH_4)_2SO_4$, NH_4HSO_4, and H_2SO_4 particles as a function of relative humidity. D_{P0} is the diameter of the particle at 0% RH [19]. . . . 5

6.1 ATB height profiles at the 15th of October in 2014. . . . 9
6.2 RH and ATB at 200 meter and ANC (diameter = 9.37 - 516 nm) at 60 meter at the 15th of October in 2014. . . . 10
6.3 Available AOD from AERONET website at the 15th of October in 2014 [5]. . . . 11
6.4 Correlation between RH and ATB at the 15th of October in 2014. The ATB data that is used to create this plot are the 10 minute averages. . . . 11
6.5 $f_{\beta_{att}}(RH)$ as function of relative humidity below 100% (blue dots) at 200 meter and its Hänel function fit (red line) on the 15th of October 2014. . . . 12
6.6 ATB height profiles at the 25th of October in 2014. . . . 12
6.7 RH and ATB at 200 meter and ANC (diameter = 9.37 - 516 nm) at 60 meter at the 25th of October in 2014. . . . 13
6.8 Correlation between RH and ATB at the 25th of October in 2014. The ATB data that is used to create this plot are the 10 minute averages. . . . 14
6.9 $f_{\beta_{att}}(RH)$ as function of relative humidity below 100% (blue dots) at 200 meter and its Hänel function fit (red line) on the 25th of October 2014. . . . 14
6.10 ATB height profiles at the 10th of November in 2014. . . . 15
6.11 RH and ATB at 200 meter and ANC (diameter = 9.37 - 516 nm) at 60 meter at the 10th of November in 2014. . . . 16
6.12 Available AOD from AERONET website at the 10th of November in 2014 [5]. . . . 17
6.13 Correlation between RH and ATB at the 10th of November in 2014. The ATB data that is used to create this plot are the 10 minute averages. . . . 17
6.14 $f_{\beta_{att}}(RH)$ as function of relative humidity below 100% (blue dots) at 200 meter and its Hänel function fit (red line) on the 10th of November 2014. . . . 18
6.15 ATB height profiles at the 13th of October in 2014. . . . 19
6.16 RH and ATB at 200 meter and ANC (diameter = 9.37 - 516 nm) at 60 meter at the 13th of October in 2014. . . . 20
6.17 ATB height profiles at the 25th of October in 2014. . . . 21
6.18 RH and ATB at 200 meter and ANC (diameter = 9.37 - 516 nm) at 60 meter at the 25th of October in 2014. . . . 22
6.19 ATB height profiles at the 30th of October in 2014. . . . 23
6.20 RH and ATB at 200 meter and ANC (diameter = 9.37 - 516 nm) at 60 meter at the 30th of October in 2014. . . . 24
6.21 ATB height profiles at the 4th of November in 2014. . . . 25
6.22 RH and ATB at 200 meter and ANC (diameter = 9.37 - 516 nm) at 60 meter at the 4th of November in 2014. . . . 26
6.23 ATB height profiles at the 12th of November in 2014. . . . 27
6.24 RH and ATB at 200 meter and ANC (diameter = 9.37 - 516 nm) at 60 meter at the 12th of November in 2014. . . . 28

1 Abstract

Clouds and aerosols continue to contribute to the largest uncertainty to estimates and interpretations of the Earth's changing energy budget. By comparing relative humidity (RH) and attenuated backscatter ratio (ATB) data and deriving scattering hygroscopic enhancement factors at the Cabauw Experimental Site for Atmospheric Physics Research (CESAR), an attempt is made to better understand the process of aerosol hygroscopic growth. This is done by ground based ceilometer, hygrometer and SMPS technology gathering data during the ACCEPT campaign in 2014, resulting in a high temporal resolution, continuous measurements and the possibility to compare the data with ancillary information measured on the same location. Some aerosol number concentration (ANC) data is also taken into account as indication of the influence of ANC on ATB. For the three studied time intervals with a large variation (>30%) in RH, a convincing relation between RH and ATB is found, which can be linked to the Köhler curve when a direct relation between aerosol size and ATB is assumed. For these three time intervals, scattering hygroscopic enhancement factors are derived with similar γ values as reported in previous studies. Further research is required to analyze the correlation between RH and ATB more and rule out other influences on ATB.

2
Introduction

Clouds and aerosols continue to contribute to the largest uncertainty to estimates and interpretations of the Earth's changing energy budget [4]. The influence of a factor that can cause climate change is therefore often evaluated in terms of its radiative forcing. In the Third Assessment Report of the International Panel on Climate Change (IPCC), aerosol radiative forcings are split into direct and indirect effects. Scattering and absorbing of radiation by aerosols is called the direct effect, which leads to a cooling or warming effect respectively. The indirect effect is the mechanism by which aerosols modify micro-physical cloud properties resulting in changes in the radiative properties, coverage and the lifetime of clouds [14]. Aerosol act as tiny 'seeds' on which water vapor condenses and cloud droplets are formed. The aerosols that are involved in cloud formation are called cloud condensation nuclei (CCN). An increase in aerosol concentration can increase the number of available CCN and thus cause a larger number of cloud droplets but with a smaller size. One of the effects of this phenomenon is called the 'cloud albedo effect' [13], as more droplets with a smaller size increase the cloud albedo [23]. Another effect is the so-called 'cloud lifetime effect' [13], which includes micro-physical changes in the liquid water content, cloud height and lifetime [14]. An increase in albedo generates a cooling effect on climate [6] and represents the major source of uncertainty in assessing the global radiative forcing [4]. This high degree of uncertainty can be reduced through a better understanding of hygroscopic growth of aerosols, which is the capacity of aerosols to pick up water from the environment and increase in size.

The hygroscopicity of aerosols is determined by their chemical composition. Aerosols with a higher hygroscopicity are more sensitive to changes in RH. Hygroscopic growth of aerosols resulting from a rising RH then results in additional light being scattered, among other effects [21].

Many studies have investigated the effect of hygroscopic growth with a changing RH [7, 11, 22, 28]. The main drawbacks of the previously used methods are the modification of ambient conditions, a low temporal resolution, possible radiosonde drift and omitting coarse mode aerosols, while they can have a significant effect on scattering enhancement factors [27].

In this work, hygroscopic growth of aerosols is analyzed with RH and ATB data. An attempt is made to find a relation between RH and ATB by comparing big variations (>30%) in RH with the corresponding ATB data and by applying the scattering hygroscopic enhancement factor. This scattering hygroscopic enhancement factor is one of the physical parameters commonly applied to describe aerosol hygroscopicity [9]. The used data is collected at the Cabauw Experimental Site for Atmospheric Physics Research (CESAR), where a Vaisala LD40 Ceilometer lidar system and a meteorological tower including hygrometer are present. Datasets acquired specifically during the ACCEPT (Analysis of the Composition of mixed-phase Clouds with extended Polarization Techniques) campaign in October and November of 2014 are used. This instrumental setup and data selection has the benefits of a high temporal resolution, can measure continuously and has the possibility to compare the data with ancillary information that is produced on the same location (like aerosol number concentration, aerosol chemical composition or wind direction) [8].

The remainder of this thesis is organized as follows: chapter 3 describes the theoretical background of the research question. In chapter 4, information is provided on the measurement devices at the CESAR Observatory. Chapter 5 discusses the data selection and handling. After the results of both the RH and ATB comparison and the scattering hygroscopic enhancement factor in chapter 6, the paper finishes with conclusions and recommendations.

3
Theoretical Background

3.1. Atmospheric aerosols

Aerosols are tiny particles and liquid droplets present in the air. Our atmosphere contains significant concentrations of aerosol particles, sometimes as high as $10^7 - 10^8 cm^{-3}$. The diameters of these particles span over four orders of magnitude, from a few nanometers to around $100\mu m$. The number of aerosols in the atmosphere decreases rapidly with their size [19], as can be seen in Figure 3.1 for a typical example of aerosol size information.

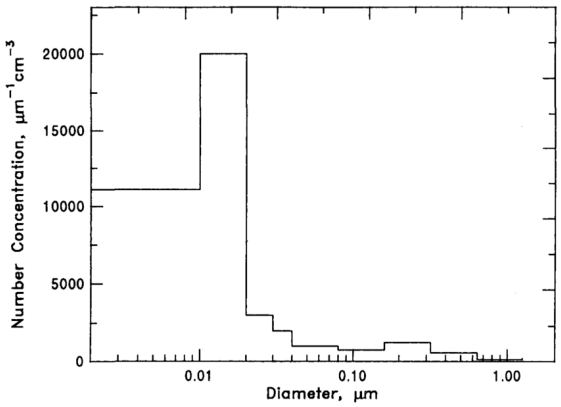

Figure 3.1: Aerosol number concentration normalized by the width of the size range against the logarithm of the diameter for a typical example of aerosol size information [19].

Aerosols can be either primary or secondary, depending on whether they are emitted into or are formed in the atmosphere [12]. The bulk of aerosols - about 90% by mass - have a natural origin. The largest natural source of primary aerosols are salt particles, evaporating from the oceans. Other natural primary aerosols are dust blown from deserts, biological aerosols (like seeds, pollen and spores) and volcanoes. The other 10% of aerosols have an anthropogenic source, including incinerators, agriculture, mining and transportation. Though less abundant than natural forms, anthropogenic aerosols can dominate the air downwind of urban and industrial areas [25].

Such a polluted situation can occur at CESAR for example when a high pressure system over The Netherlands block incoming fronts, resulting in a stable and polluted atmosphere. This meteorological situation has occurred in May 2008 and is studied by multiple research groups [6, 10]. In another work, aerosol chemical composition was analyzed for a year (2007 - 2008) at five monitoring stations spread over The Netherlands. The main components of aerosols in PM2.5 (particulates with an aerodynamic diameter smaller than 2.5 μm) were: 42-48% secondary inorganic aerosol (ammonic nitrate and ammonic sulphte), 22-37% carbonaceous substances, 8% marine salt and 5% mineral dust and metals. The coarse mode had more marine salt and metal which resulted in a more balanced contribution of these four sources [26]. Morgan et al. has also studied the aerosol chemical distribution at the CESAR station in May 2008 and reported that aerosols were mainly comprised of ammonic nitrate and organic matter [17]. In this paper, not much attention will be given to the chemical composition, as clouds are more sensitive to the size and number of aerosols particles present in the atmosphere than to their chemical composition [2].

As stated in the introduction, aerosols and clouds continue to contribute to the largest uncertainty to estimates and interpretations of the Earth's changing energy budget [4]. This radiative balance controls the Earth's surface temperature. The influence of a factor that can cause climate change is therefore often evaluated in terms of its radiative forcing. In the Third Assessment Report of the International Panel on Climate Change (IPCC), aerosol radiative forcings are split into direct and indirect effects.

3.1.1. Aerosol-Solar Radiation Interactions: Direct Effect

Scattering and absorbing of radiation by aerosols is called the direct effect of aerosols, which leads to a cooling or warming effect respectively. Different aerosols scatter or absorb radiation to varying degrees, depending on their physical properties. In addition to scattering or absorbing radiation, aerosols can alter the albedo of the planet, depending also on the reflectivity of the land beneath the aerosols. Aerosols are not distributed evenly around the planet, adding to the complexity of analyzing the overall effect of aerosols on the climate [25].

In the atmosphere, scattering can happen in two different ways, depending on the size of the particle scattering the light. Raleigh scattering occurs when the particles are considerably smaller than the wavelength of the light being scattered. This type of scattering is more effective at short wavelengths, as it is strongly inversed wavelength dependent. Most aerosols however are bigger than the wavelength of light resulting in Mie scattering. Mie scattering produces a pattern like an antenna lobe, with a sharper and more intense forward lobe for larger particles, as opposed to Rayleigh scattering that produces scattering more evenly spread in all directions. Mie scattering is not strongly wavelength dependent and therefore reflects all wavelengths more evenly, resulting in whiter light [19].

3.1.2. Aerosol-Solar Radiation Interactions: Indirect Effect

The indirect effect of aerosols is the mechanism by which aerosols modify micro-physical cloud properties resulting in changes in the radiative properties, coverage and the lifetime of clouds [14]. In Earth's atmosphere, cloud droplet do not form by condensation of water molecules in the absence of a foreign condensation nucleus. This would require the initial formation of very small droplets with a very small radius of curvature. Fundamental thermodynamics shows that the equilibrium vapor pressure over such a strongly curved surface is always much greater than that over a flat surface, as shown by the blue line in Figure 3.2 [20]. This is called the 'Kelvin effect' and is the reason why most clouds owe their existence to aerosols. These aerosols, cloud condensation nuclei (CCN), function as tiny 'seeds' by providing a larger initial radius that preventing immediate evaporation of the water. CCN that dissolve in water also profit from the 'Raoult effect', namely the fact that solutions evaporate water molecules at a slower rate than pure water does. The two opposing effects of curvature and solute can be combined into one equation, namely the Köhler equation. The Köhler curve for several chemicals is given in Figure 3.2 [20]. Plot b. highlights the two opposing effects of evaporation and condensation. When the air has a known RH (e.g. 100.3%), two things can happen. If $RH_{droplet} > RH_{air}$, the droplet evaporates until RH_{air} is reached. This is from the point the Köhler curve first hits RH_{air} until the second time it hits RH_{air}. If $RH_{droplet} < RH_{air}$, the droplet grows due to condensation. This can result in discontinued aerosol growth when RH_{air} is first reached, or in extra droplet growth when the second RH_{air} is passed. Activated droplets such as these continue growing until they consume the excess humidity (driving RH_{air} down towards 100%) [20].

As aerosols are mostly classified by size, the classification of CCN is given in Table 3.1 [20].

Classification	**Radius** (μm)
Ultrafine aerosols	$0.001 - 0.01$
Fine aerosols	$0.01 - 1$
Coarse mode aerosols	$1 - 10$

Table 3.1: Classification of cloud condensation nuclei (CCN) aerosols by radius (μm) [20].

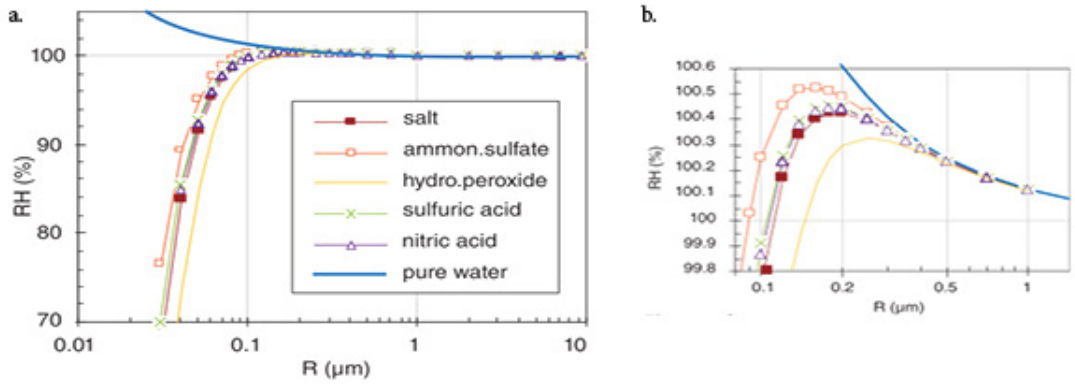

Figure 3.2: **a.** Köhler curve, showing equilibrium relative humidities over droplets of different radius with various solutes. T = 0°C. Solute mass = 10^{-16} g. **b.** Blow-up of Figure a, highlighting the two opposing effects of evaporation and condensation [19].

An increase in aerosol concentration can increase the number of available CCN and thus create a larger number of cloud droplets but with a smaller size. One of the effects of this phenomenon is called the 'cloud albedo effect' [13], as more droplets with a smaller size increase the cloud albedo [23]. Another effect is the so-called 'cloud lifetime effect' [13], which includes micro-physical changes in the liquid water content, cloud height and lifetime [14]. An increase in albedo generates a cooling effect on climate [6] and represents the major source of uncertainty in assessing the global radiative forcing [4]. This high degree of uncertainty can be reduced through a better understanding of hygroscopic growth of aerosols.

3.2. Hygroscopicity

Hygroscopicity is the capacity of aerosol to pick up water from the environment and increase in size. The hygroscopicity of aerosols is determined by their chemical composition. Most inorganic aerosols are hygroscopic, sulfuric acid particles are always hydrated, but salts exist as dry particles at sufficiently low RH and experience an abrupt uptake of water at their specific RH of deliquescence (DRH). However, salt solutions (e.g. $(NH_4)_2SO_4$) generally do not crystallize at DRH but remain supersaturated until a much lower RH. This difference in deliquescence and crystallization point is called a hysteresis phenomenon and is shown in Figure 3.3 [19].

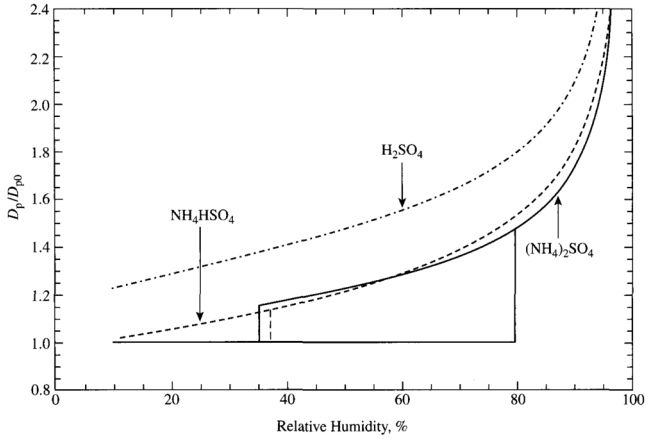

Figure 3.3: Diameter change of $(NH_4)_2SO_4$, NH_4HSO_4, and H_2SO_4 particles as a function of relative humidity. D_{P0} is the diameter of the particle at 0% RH [19].

Highly hygroscopic aerosols (f.e. H_2SO_4) do not exhibit this deliquescent behavior. The water content associated with these chemicals changes smoothly as the RH increases or decreases, shown in Figure 3.3 [19]. Hygroscopic aerosols can grow small droplets even at RH < 100%, as they attract water vapor out of the air [20].

3.2.1. Measuring hygroscopicity

Hygroscopic growth of aerosols has been studied extensively, and physical laws have been established empirically between relative humidity and aerosol optical parameters [7].
Atmospheric RH alters the optical and microphysical properties of atmospheric aerosols due to aerosol hygroscopic growth. For example, the mass scattering efficiency (how efficient aerosols can scatter light) of aerosol particles depends on the particle size and refractive index. The refractive index is in turn determined by the chemical composition of the aerosol [18]. On the other hand, the refractive index decreases with increasing RH. However, this decrease is not large enough to counteract the increase in cross section. Thus, the size dependence dominates, leading to an increase in scattering as RH increases, among other effects [9, 21].
Hygroscopic growth can be measured in multiple ways. Two ways that are used in this paper are elaborated upon in the following sections, namely by analyzing the lidar attenuated backscatter ratio and by applying the scattering hygroscopic enhancement factor.

Lidar attenuated backscatter ratio

One of the scattering properties of aerosols that can be measured from the ground is the attenuated backscatter ratio (ATB). ATB is the fraction of scattered intensity that is redirected into the backward hemisphere of the scattering particle, which can be measured using lidar techniques (more on the used equipment in chapter 3).
ATB is not only dependent on aerosol size, but also on chemical composition and aerosol number concentration (ANC). In this paper, the chemical composition of the analyzed aerosols is not taken into account but an estimation of the influence of ANC on ATB is made. By comparing ATB data with RH, an attempt is made to better understand the process of aerosol hygroscopic growth. This comparison is made for 8 time intervals in this paper, of which 3 time intervals that have a large drop or rise in RH (>30%) and 5 time intervals with a flat RH (<10% drop or rise).

Scattering hygroscopic enhancement factor

Another way of describing hygroscopic growth is by determining the hygroscopic growth function $f(RH)$ as defined in Equation 3.1,

$$f(RH) = \frac{1 - RH}{1 - RH_{dry}}^{-\gamma} \tag{3.1}$$

with a reference value RH, RH_{dry} where no hygroscopic growth is expected and γ, an empirical fitting parameter. This hygroscopic growth function, also called the Hänel function, is one of the physical parameters commonly applied to describe aerosol hygroscopicity [9].
To derive a value for the empirical fitting parameter γ, the hygroscopic growth function for the attenuated total backscatter coefficient $f_{\beta_{att}}(RH)$ has to be plotted against RH and fitted for Equation 3.1. $f_{\beta_{att}}(RH)$ is defined as

$$f_{\beta_{att}}(RH) = \frac{\beta_{att}(RH)}{\beta_{att}(RH_{dry})} \tag{3.2}$$

with a reference value RH, RH_{dry} where no hygroscopic growth is expected and β_{att} the attenuated total backscatter coefficient.
In this paper, the hygroscopic backscattering enhancement factor is derived for the 3 selected days with a largely varying RH (>30%).

4

Observations from CESAR Observatory

4.1. General description of the CESAR Observatory

All analyzed data was collected at the CESAR (Cabauw Experimental Site for Atmospheric Physics Research) Observatory, located in the Netherlands (51.971° N, 4.927° E). The observatory is located 0.7 m below the mean sea level and is equipped with a large set of instruments providing constant measurements for the study of the atmosphere. The site is representative for North-West Europe and features continental and maritime conditions, depending on the wind direction. The CESAR Observatory is run by the Royal Netherlands Meteorological Institute (KNMI), De Bilt, The Netherlands [1, 3, 16].

4.2. Instrumentation

Many studies have investigated the effect of hygroscopic growth with a changing RH [7, 11, 22, 28]. Some experimental studies were carried out using in-situ measurement techniques or under controlled laboratory conditions that modify the ambient conditions of the sample [11, 22]. Other studies use the synergy of lidars and radiosondes [7], which results in a low temporal resolution and possibly suffer from radiosonde drift [15]. Yet others use Humidified Tandem Differential Mobility Ananlyzer (H-TDMA) size distribution data to estimate the dependence of aerosol light-scattering properties with RH (the scattering enhancement factor) [28]. The main drawback of this method is that it does not include coarse mode aerosols, while they can have a significant effect on scattering enhancement factors [27].

In this work, hygroscopic growth of aerosols is analyzed by comparing RH and ATB data. The RH is measured in the CESAR meteorological tower using a hygrometer at a height of 200 meter and with a time resolution of 10 minutes. The ATB data is provided by a Vaisala LD-40 Ceilometer, a lidar (Light Detection and Ranging) based instrument. The ceilometer operates at a wavelength of 855 nm with a time resolution of 15 seconds and a spatial (vertical) resolution of 7.5 meter [24]. Heights up to 1800 meter are taken into account, measurements at a height of 200 meter are compared with the RH data. Aerosol number concentration (ANC) plots shown in this paper are constructed using data from the CESAR Scanning Mobility Particle Sizer (SMPS), TSI Model 3034. The SMPS operates at a height of 60 meter and has a time resolution of 1 hour. The SMPS data used refers to particles with diameters between 9.37-516 nm. When available, aerosol optical depth (AOD) plots are retrieved from the AERONET (Aerosol Robotic Network) website. These AODs are measured using a sun photometer [5]. This instrumental setup has the benefits of a hight temporal resolution, continuous measurements and the possibility to compare the data with ancillary information produced on the same location [8].

4.3. ACCEPT campaign

The ACCEPT (Analysis of the Composition of mixed-phase clouds with Extended Polarization Techniques) campaign was performed at the CESAR Observatory in 2014. This campaign ran from the 6th of October to the 16th of November and was focused on mixed-phase clouds. No data of the actual ACCEPT campaign was used but by using only data collected during these 42 days, more and different data is available for future (follow-up) studies.

5
Methodology

5.1. Data selection

In order to see a clear pattern between RH and ATB, 8 time intervals are selected from the 42 ACCEPT campaign days with a drop or rise of 30% or more in RH. These big drops and rises are compared with the changes in ATB. From these 8 time intervals, 5 time intervals are discarded because of saturated or very low ATB signals, which made the interpretation of the results difficult.
In order to analyze the relation between the RH and the ATB, it is important to take into account other factor that can influence ATB. First of all, a control group is composed by scanning all 42 ACCEPT campaign days for periods of time with RH levels not changing more than approximately 10%. The data of these so-called 'flat RH days' are then compared with the corresponding ATBs. From these 9 days, 4 are discarded because of saturated or low backscatter signals, which again made the interpretation of the results difficult.
Since the ATB depends both on the size of the particles (due to water uptake) and the number of particles (ANC), a constant ANC has to be ensured to support a relation between ATB and RH. So in the second step of the analysis, data from the SMPS instruments were examined. The data used from this SMPS has a diameter between 9.37-516 nm. As far as there were data available for the selected days, aerosol optical depth (AOD) is used as another measure of the amount of aerosols in the atmosphere. AOD plots are retrieved from the AERONET (Aerosol Robotic Network) website and is measured using a sun photometer [5].

5.2. Data processing

As the ATBs were given every 15 seconds and sometimes returned very low values, all ATBs are averaged over 5 as well as 10 minutes. This is done by computing the average for every 5 and 10 minute time interval of the ATB and time data. For the comparison of the ATB and the RH data, the 5 minute averages are used. For the ATB versus RH graphs, 10 minute averages are used, as RH is measured every 10 minutes.
Scattering hygroscopic enhancement factors are derived for the three time intervals with a large variation in RH (>30%). All RH data >100% is discarded here in order fit a sensible scattering hygroscopic enhancement factor. As all RH values lie above RH = 60%, the lowest RH value per day is used as RH_{dry}. For these plots, also the 10 minute ATB averages are used, as RH is measured every 10 minutes.

6 Results and Discussion

6.1. Lidar attenuated backscatter ratio: Case studies with variable RH

In order to see a clear pattern between RH and ATB, time intervals on 3 days with a drop or rise of 30% or more in RH are selected, namely the 15th and 25th of October and the 10th of November.
For every day, first ATB height profiles are given to show the overall atmospheric situation that day. This is followed by a ATB and a RH plot at a height of 200 meter to analyze the correlation. The ANC for aerosols with diameters between 9.37-516 nm for these days is then provided. When available, aerosol optical depths (AOD) from the AERONET (Aerosol Robotic Network) website are also mentioned as another indication of the influence of changing numbers of aerosols on ATBs. The relation between RH and ATB is shown in a concluding plot. Lastly, the hygroscopic growth function is used to fit the scattering hygroscopic enhancement factor.

6.1.1. 15th of October

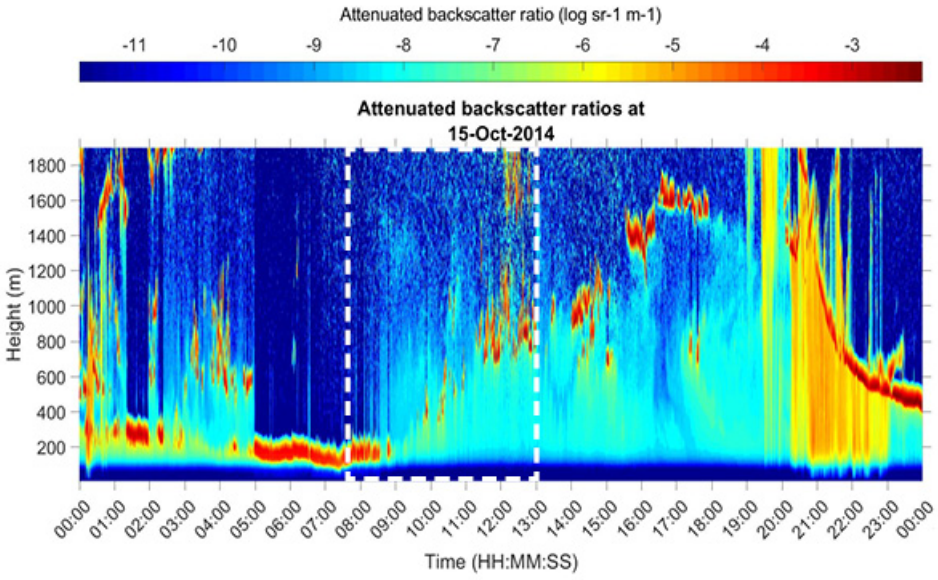

Figure 6.1: ATB height profiles at the 15th of October in 2014.

A general overview of the ATBs during this day is given in Figure 6.1. The time interval for which the RH drops >30% is indicated in the figure with a white rectangle. Signals after 19:00 can't be used to draw any conclusions as the ATB is saturated.

In Figure 6.2 a. and b., the RH and ATB at 200 meter are compared. ANC for aerosols with diameters between 9.37-516 nm are also provided to give an indication of the influence of ANC on the ATB. The RH in the selected time interval drops from over 100% to around 70%. The ATB also drops in this time interval. The biggest drop in ATB is observed during the first two hours, while the RH drops fairly constant during this time interval.

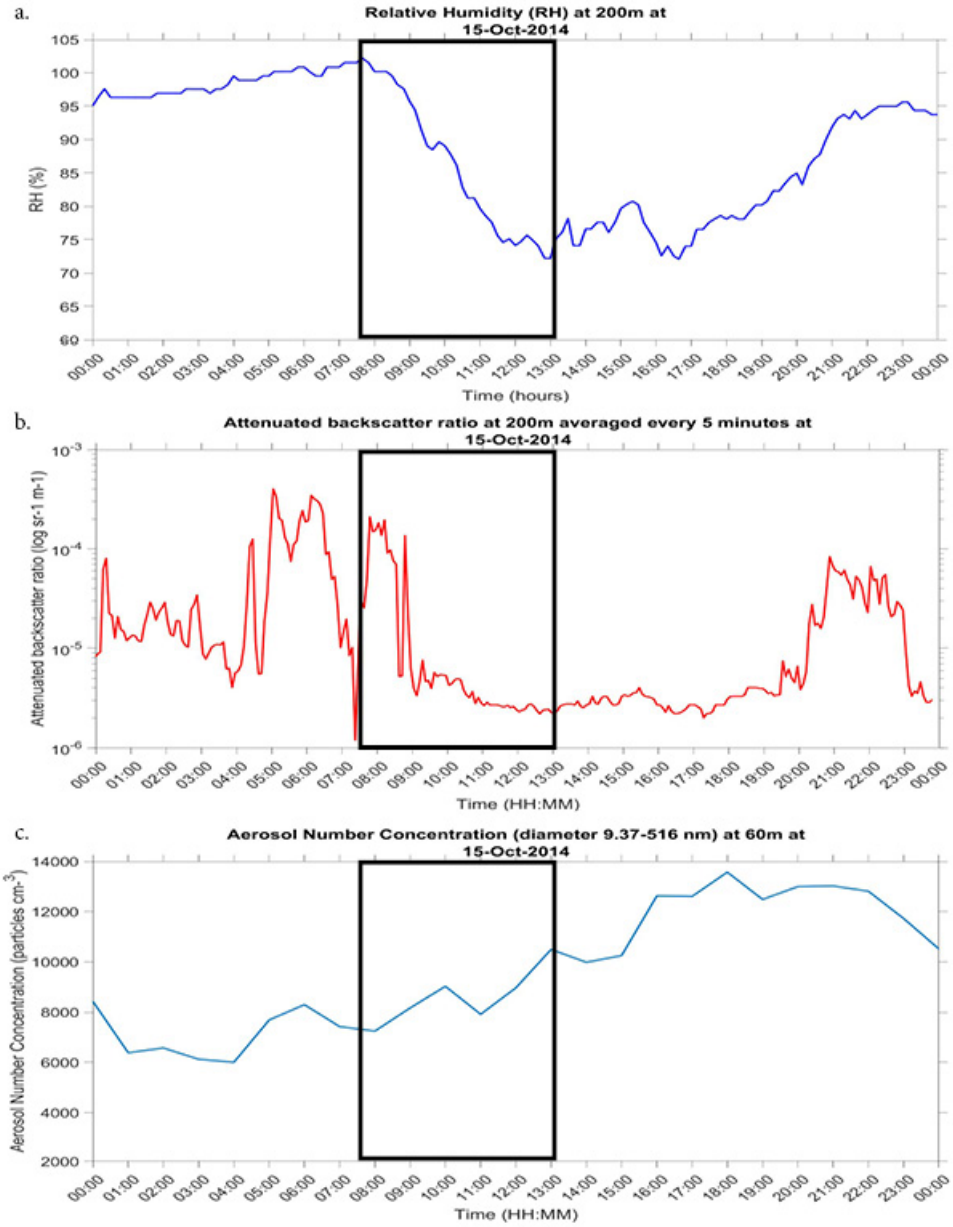

Figure 6.2: RH and ATB at 200 meter and ANC (diameter = 9.37 - 516 nm) at 60 meter at the 15th of October in 2014.

The ATB doesn't seem to be influenced by the ANC (Figure 6.2 c.) which is mostly rising in this time interval, in contrast to the dropping ATB. AOD data from AERONET were only available between 9:10 to 9:40 and 12:30 to 13:15, as shown in Figure 6.3. The displayed values seem to be meandering around a fairly constant value of 0.2 between 9:10 and 13:15 for this day [5].

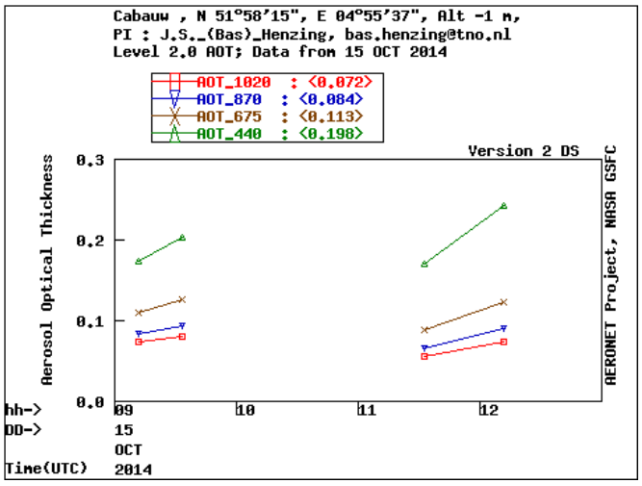

Figure 6.3: Available AOD from AERONET website at the 15th of October in 2014 [5].

The correlation between RH and ATB for the selected time interval is shown in Figure 6.4. The colors represent the passage of time, yellow being the beginning of the time interval and blue the end. A clear correlation can be found as generally the ATB is higher with a higher RH. The curve in Figure 6.4 seems to behave asymptotically towards RH = 100%. Other case studies in this paper show similar behavior.

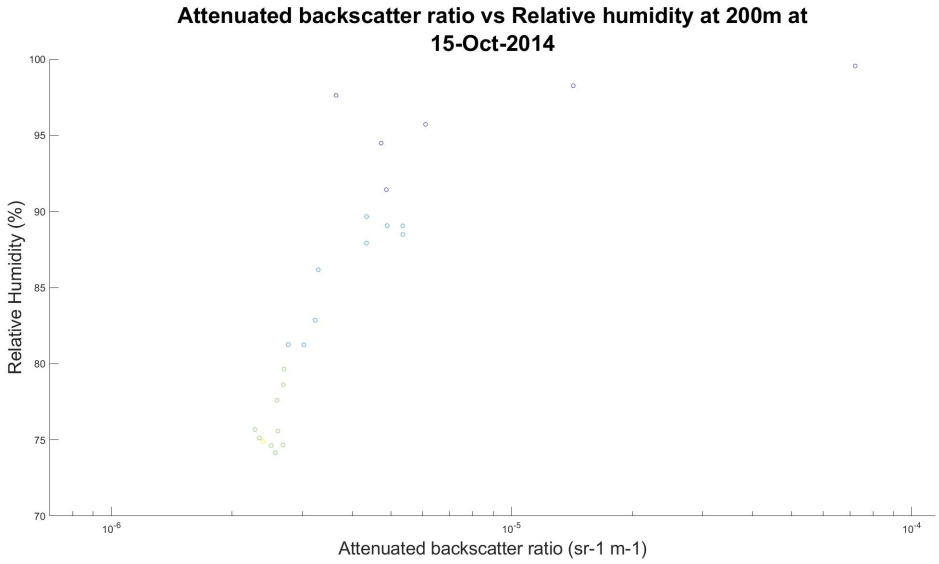

Figure 6.4: Correlation between RH and ATB at the 15th of October in 2014. The ATB data that is used to create this plot are the 10 minute averages.

In Figure 6.5, $f_{\beta_{att}}(RH)$ is plotted for all RH values below 100% (blue dots) using Equation 3.1. The Hänel function fit is produced using all other data points within the selected time interval using Equation 3.2, resulting in γ = 0.8081. For RH_{dry}, the lowest RH value for this day is used.

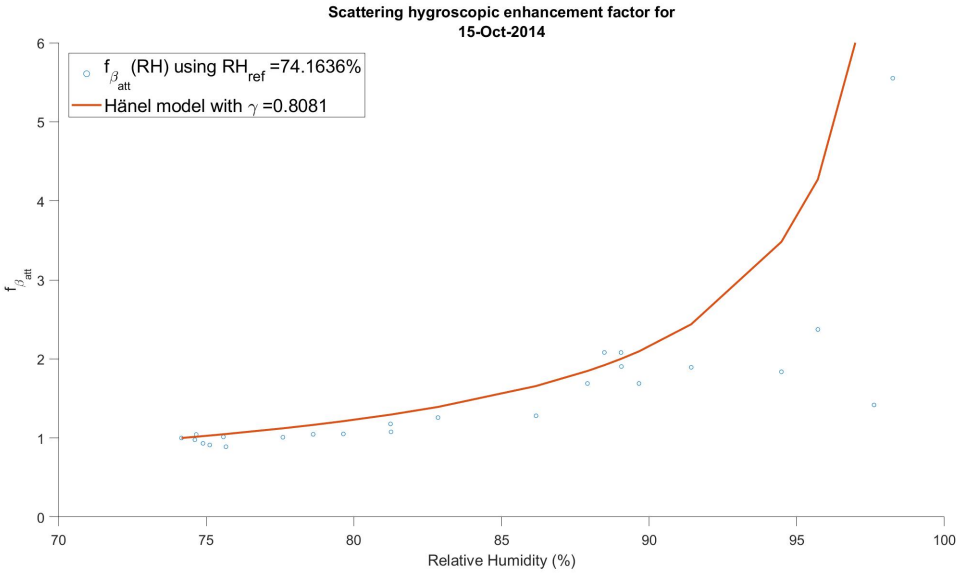

Figure 6.5: $f_{\beta_{att}}(RH)$ as function of relative humidity below 100% (blue dots) at 200 meter and its Hänel function fit (red line) on the 15th of October 2014.

6.1.2. 25th of October

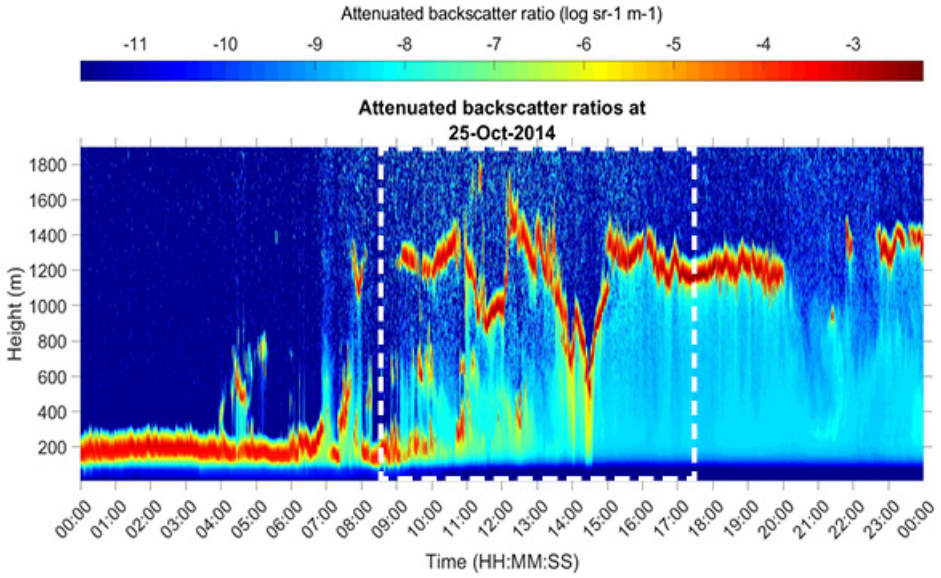

Figure 6.6: ATB height profiles at the 25th of October in 2014.

A general overview of the day is given in Figure 6.6. The time interval for which the RH drops >30% is indicated in the figure with a white rectangle.

In Figure 6.7, the RH and ATB at 200 meter are compared. ANCs for aerosols with diameters between 9.37-516 nm are also provided to give an indication of the influence of ANC on the ATB. The RH in the selected time interval drops from over 100% to around 70%. The ATB also drops in this time interval. Like the previous day, the ATB mostly drops in the first hours while the RH has its largest drop in the last few hours. The ATB is possibly influenced by the ANC as this also drops in this time interval, however the small rise in ANC in the second half of the interval is not seen in the ATB curve. AOD data from AERONET for this day is not available [5].

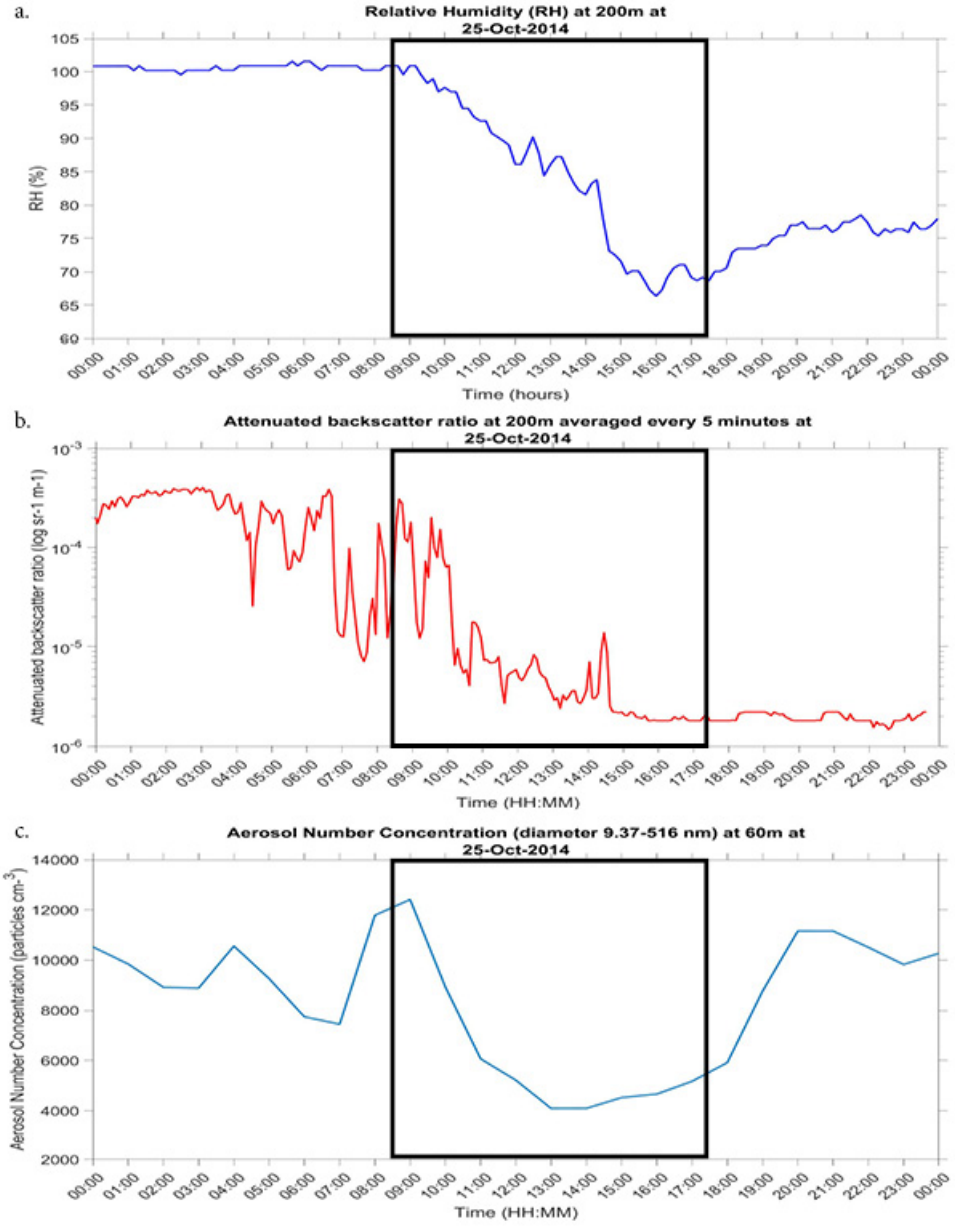

Figure 6.7: RH and ATB at 200 meter and ANC (diameter = 9.37 - 516 nm) at 60 meter at the 25th of October in 2014.

The correlation between RH and ATB for the selected time interval is shown in Figure 6.8. The colors represent the passage of time, yellow being the beginning of the time interval and blue the end. This curve shows the same correlation as the previous case as generally the ATB is higher with a higher RH and as the curve also behaves asymptotically towards RH = 100%.

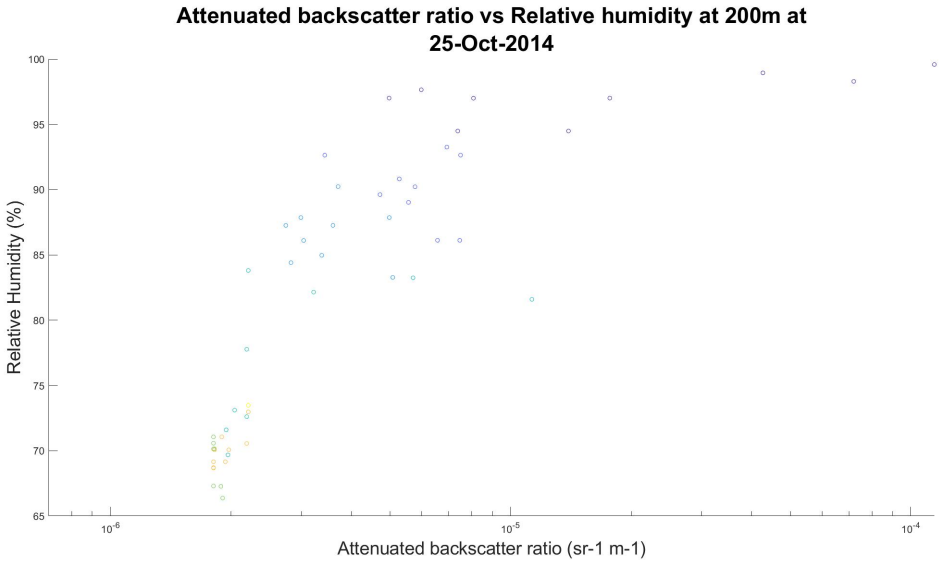

Figure 6.8: Correlation between RH and ATB at the 25th of October in 2014. The ATB data that is used to create this plot are the 10 minute averages.

In Figure 6.9, $f_{\beta_{att}}(RH)$ is plotted for all RH values below 100% (blue dots) using Equation 3.1. The Hänel function fit is produced using all other data points within the selected time interval using Equation 3.2, resulting in γ = 0.9342. For RH_{dry}, the lowest RH value for this day is used.

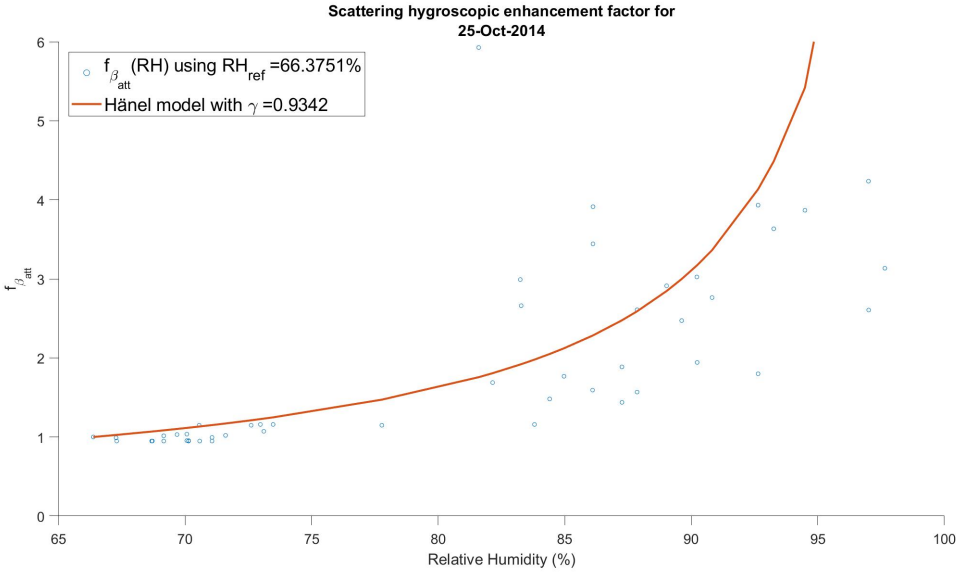

Figure 6.9: $f_{\beta_{att}}(RH)$ as function of relative humidity below 100% (blue dots) at 200 meter and its Hänel function fit (red line) on the 25th of October 2014.

6.1.3. 10th of November

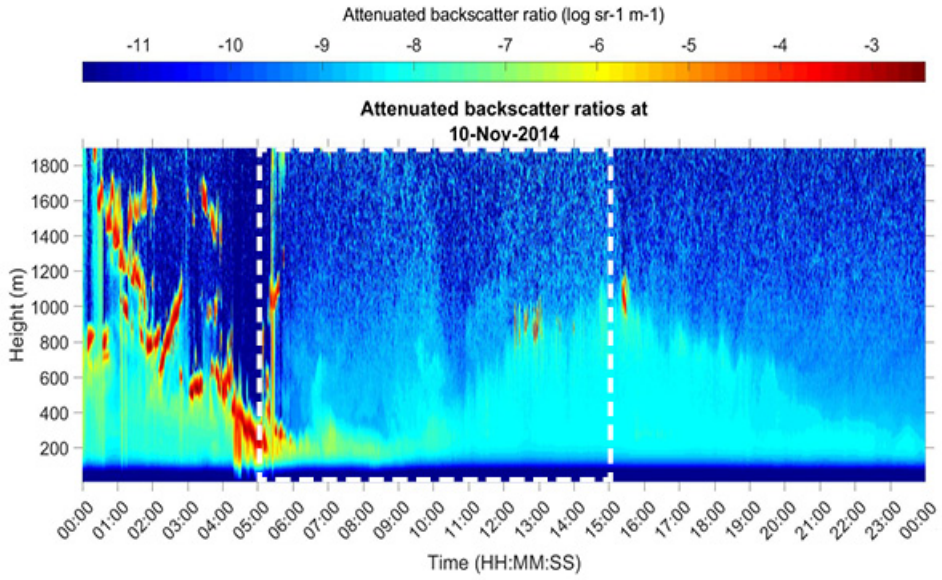

Figure 6.10: ATB height profiles at the 10th of November in 2014.

A general overview of the day is given in Figure 6.10. The time interval for which the RH drops >30% is indicated in this figure with a white rectangle.

In Figure 6.11, the RH and ATB at 200 meter are compared. The RH in the selected time interval drops from over 100% to approximately 70%. The ATB also drops in this time interval, with the biggest drop in the beginning, similar as in Figure 6.2. The ATB could be influenced by the ANC as this also drops in this time interval.

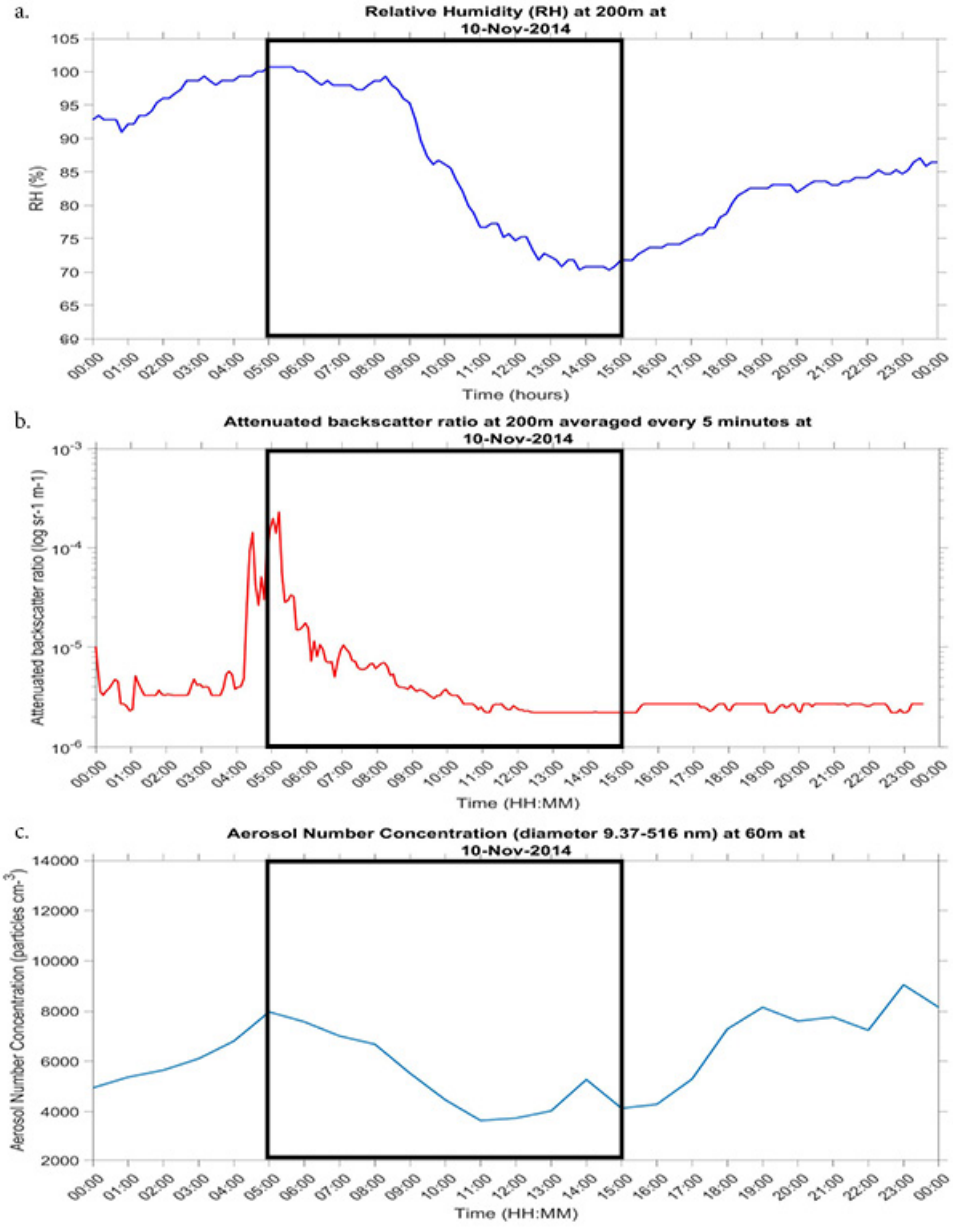

Figure 6.11: RH and ATB at 200 meter and ANC (diameter = 9.37 - 516 nm) at 60 meter at the 10th of November in 2014.

AOD data from AERONET shows a small drop (0.1) from approximately 8:30 to 10:30, followed by a larger increase (0.15) from 10:30 to 13:00 for this day [5], as can be seen in Figure 6.12. Until approximately 14:15, the AOD drops again a little. This AOD behavior isn't really observed in the ATB curve, except for the drop at the beginning. This again suggests that the ATB drop is strongly related to the drop in RH.

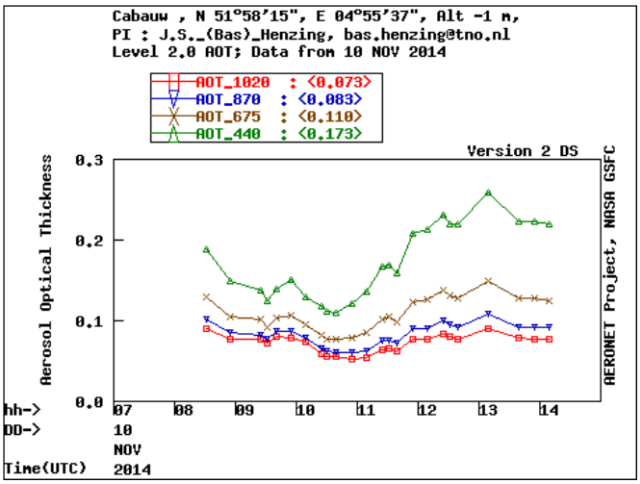

Figure 6.12: Available AOD from AERONET website at the 10th of November in 2014 [5].

The correlation between RH and ATB is shown in Figure 6.13. The colors represent the passage of time, yellow being the beginning of the time interval and blue the end. This curve shows the same correlation as seen in previous cases as generally the ATB is higher with a higher RH and as the curve also behaves asymptotically towards RH = 100%.

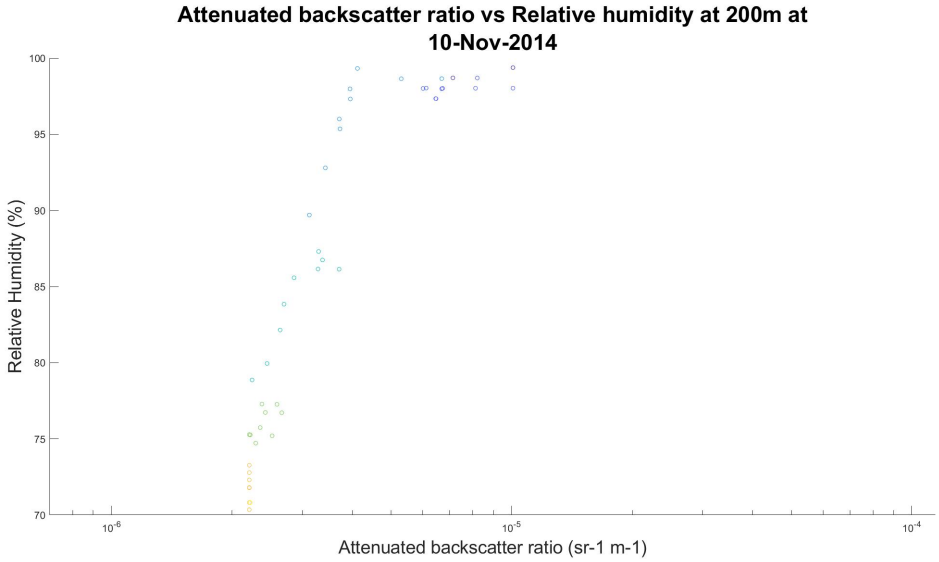

Figure 6.13: Correlation between RH and ATB at the 10th of November in 2014. The ATB data that is used to create this plot are the 10 minute averages.

In Figure 6.14, $f_{\beta_{att}}(RH)$ is plotted for all RH values below 100% (blue dots) using Equation 3.1. The Hänel function fit is produced using all other data points within the selected time interval using Equation 3.2, resulting in γ = 0.3621. For RH_{dry}, the lowest RH value for this day is used.

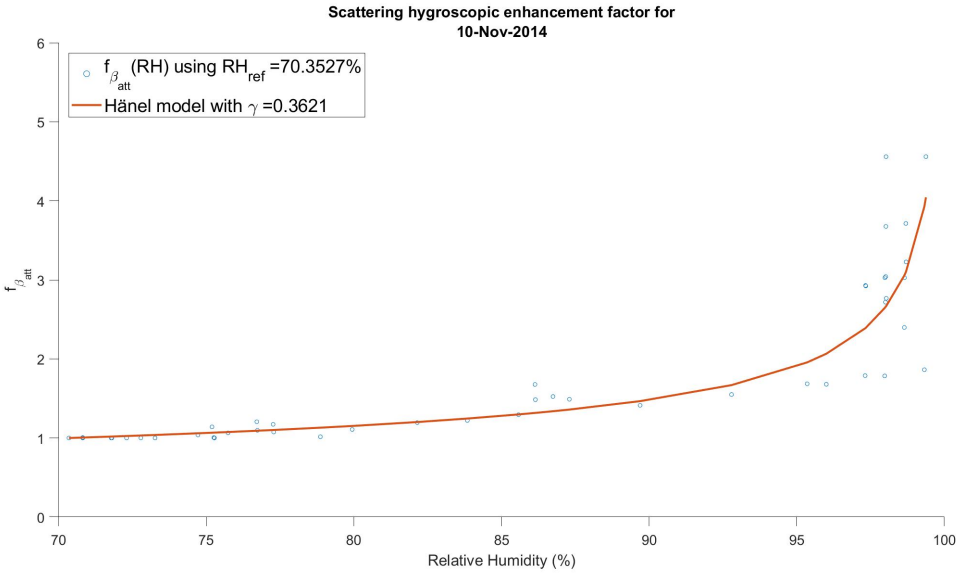

Figure 6.14: $f_{\beta_{att}}(RH)$ as function of relative humidity below 100% (blue dots) at 200 meter and its Hänel function fit (red line) on the 10th of November 2014.

6.2. Lidar attenuated backscatter ratio: Case studies with constant RH

In order to examine if significant changes in the ATB signal are observed during periods with constant RH, time intervals on 5 days with a flat RH are selected, namely the 13th, 25th and 30th of October and the 4th and 12th of November. These time intervals have a maximum change in RH of approximately 10%. For every day, first an ATB height profiles plot is shown to give a general impression of the atmospheric situation that day. This is followed by a backscatter and a RH plot at a height of 200 meter to analyze the correlation. The ANC for aerosols with diameters between 9.37-516 nm for these days is then provided to give an indication of the influence of ANC on the ATB. When available, aerosol optical depths from the AERONET website are also mentioned.

6.2.1. 13th of October

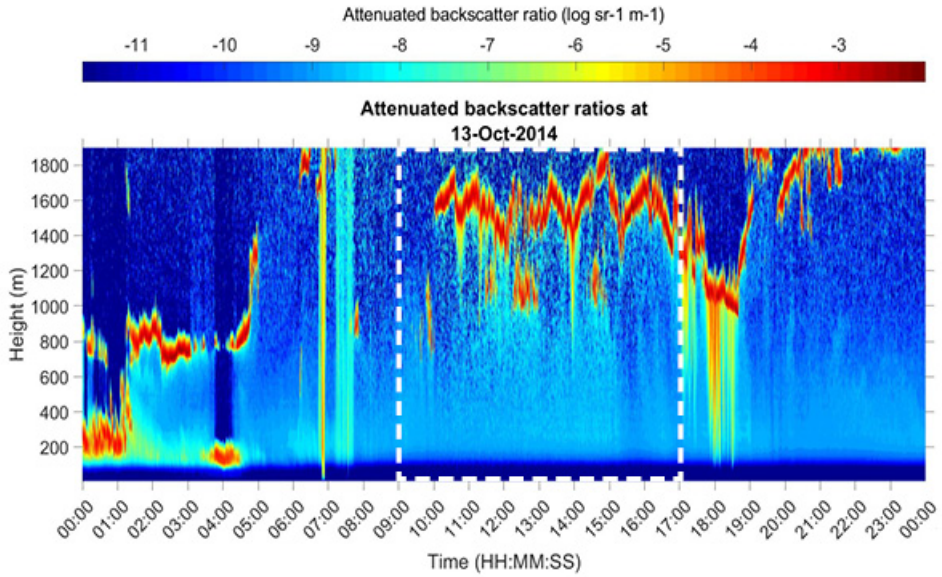

Figure 6.15: ATB height profiles at the 13th of October in 2014.

A general overview of the day is given in Figure 6.15. The time interval for which the RH stays constant (<10% variation) is indicated in this figure with a white rectangle. Signals between 6:00 and 8:00 can't be used to draw any conclusions as the ATB is saturated.

In Figure 6.16, the RH and ATB at 200 meter are compared. ANCs for aerosols with diameters between 9.37-516 nm are also provided to give an indication of the influence of ANC on the ATB. The RH in the selected time interval stays between approximately 70% and 80%. The ATB also stays fairly constant. Even though the ANC is mostly rising in this time interval, the ATB is not influenced by this change. This suggest that the flat ATB may be attributed to the fairly constant RH. There is no AOD data available from AERONET for this day [5].

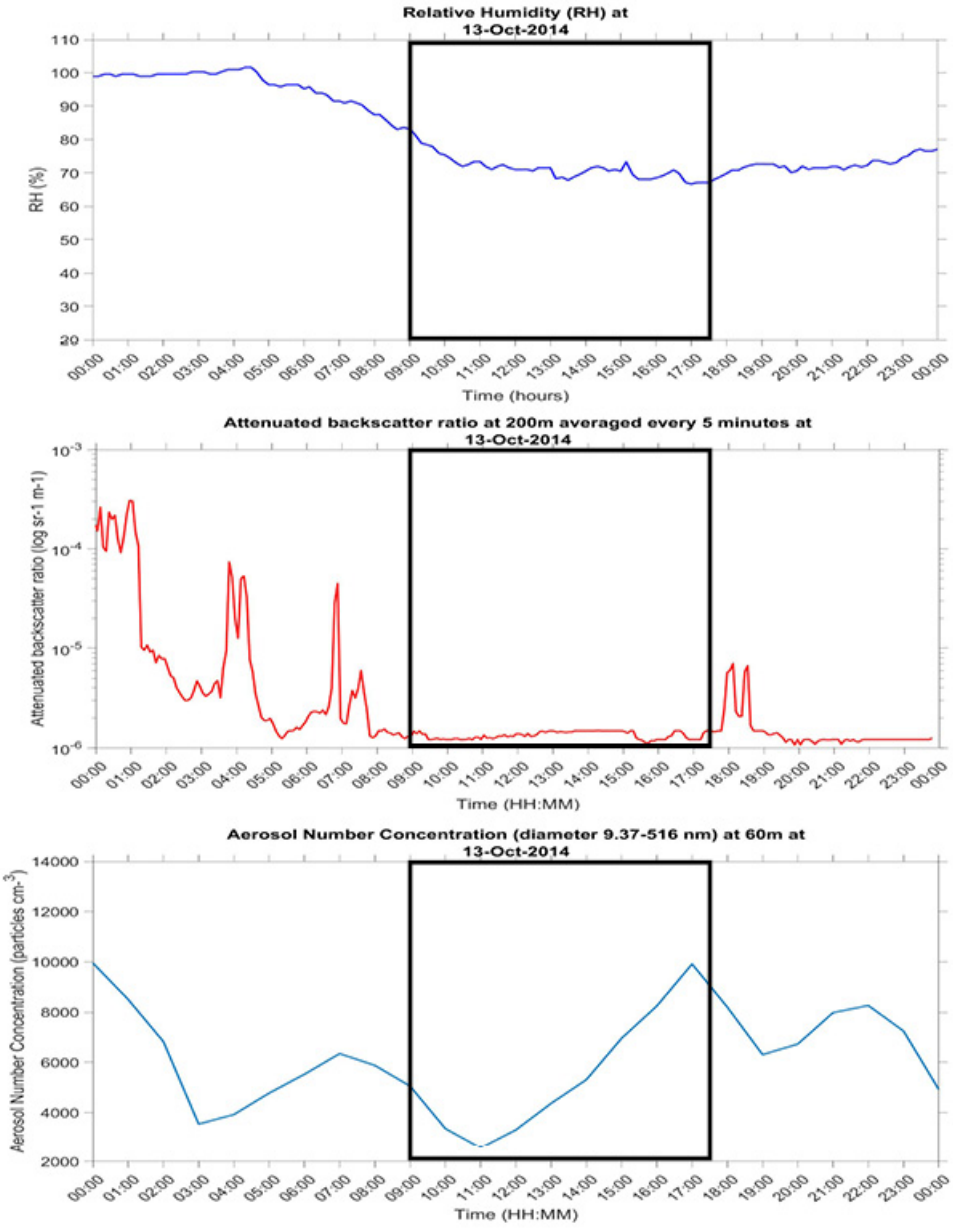

Figure 6.16: RH and ATB at 200 meter and ANC (diameter = 9.37 - 516 nm) at 60 meter at the 13th of October in 2014.

6.2.2. 25th of October

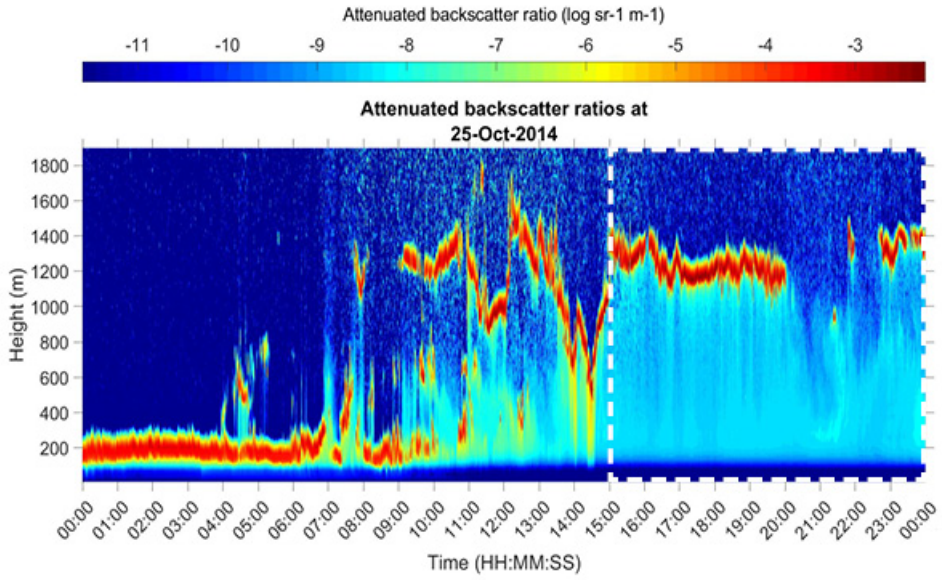

Figure 6.17: ATB height profiles at the 25th of October in 2014.

A general overview of the day is given in Figure 6.17. The time interval for which the RH stays constant (<10% variation) is indicated in the figure by a white rectangle.

In Figure 6.18, the RH and ATB at 200 meter are compared. ANCs for aerosols with diameters between 9.37-516 nm are also provided to give an indication of the influence of ANC on the ATB. The RH in the selected time interval stays approximately between around 60% to around 70%. The ATB also stays quite constant. The ATB doesn't seem to be influenced by the ANC as none of the rises and drops in ANC are seen in the ATB curve. There is no AOD data available from AERONET for this day [5].

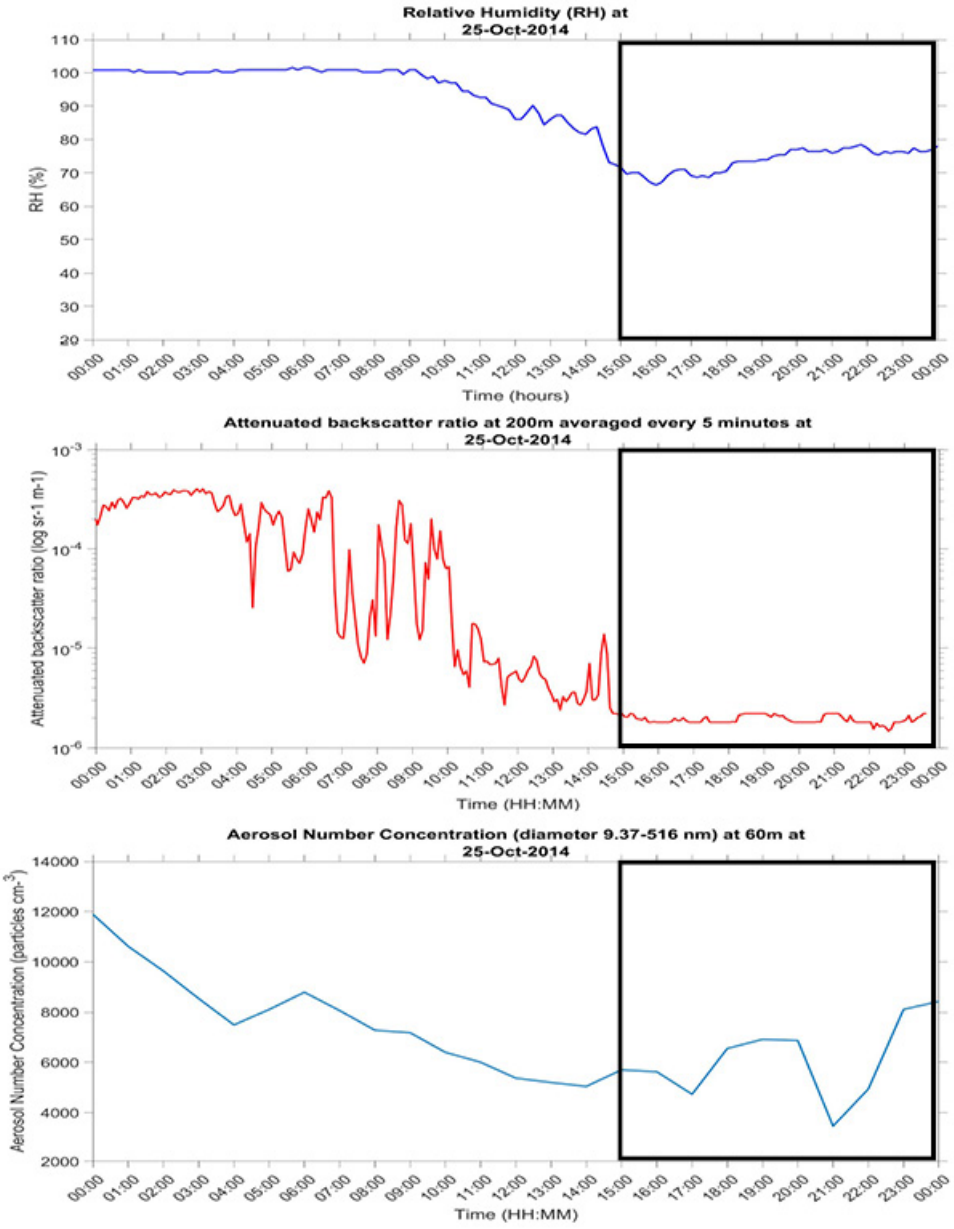

Figure 6.18: RH and ATB at 200 meter and ANC (diameter = 9.37 - 516 nm) at 60 meter at the 25th of October in 2014.

6.2.3. 30th of October

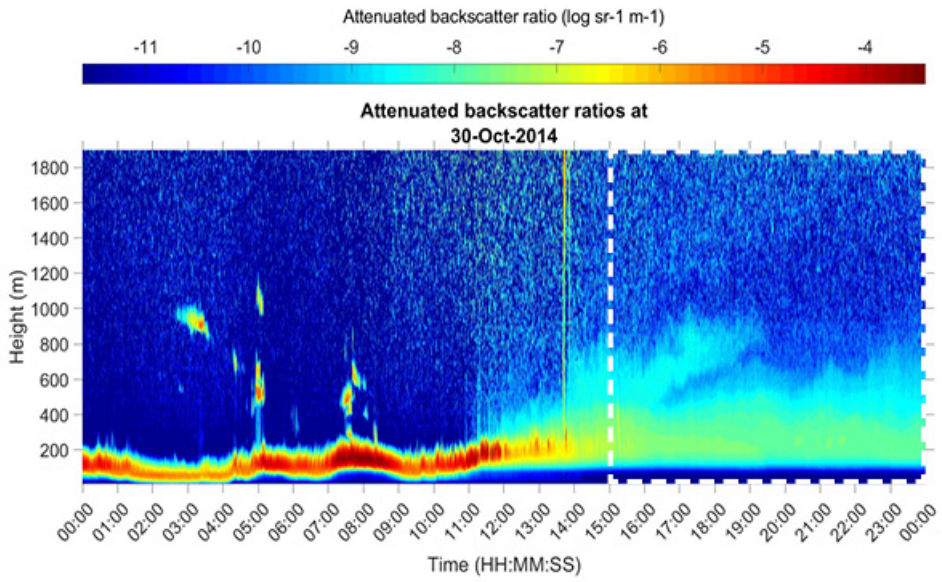

Figure 6.19: ATB height profiles at the 30th of October in 2014.

A general overview of the day is given in Figure 6.19. The time interval for which the RH stays constant (<10% variation) is indicated in this figure with a white rectangle.

In Figure 6.20, the RH and ATB at 200 meter are compared. ANCs for aerosols with diameters between 9.37-516 nm are also provided to give an indication of the influence of ANC on the ATB. The RH in the selected time interval stays approximately between 90% and 95%. The ATB also stays almost perfectly constant. The ATB doesn't seem to be influenced by the ANC as this is mostly rising in this time interval. There is no AOD data available from AERONET for this day [5].

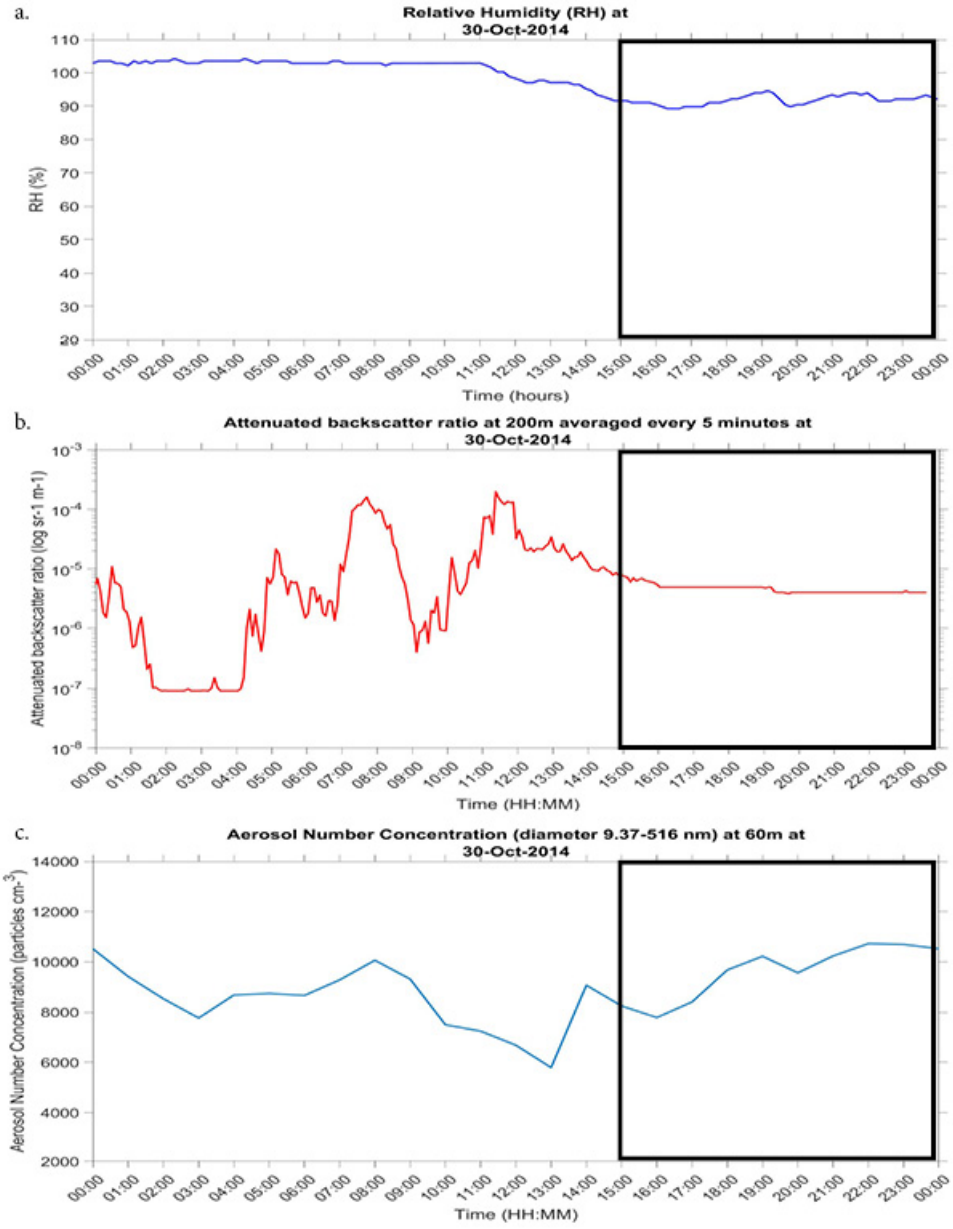

Figure 6.20: RH and ATB at 200 meter and ANC (diameter = 9.37 - 516 nm) at 60 meter at the 30th of October in 2014.

6.2.4. 4th of November

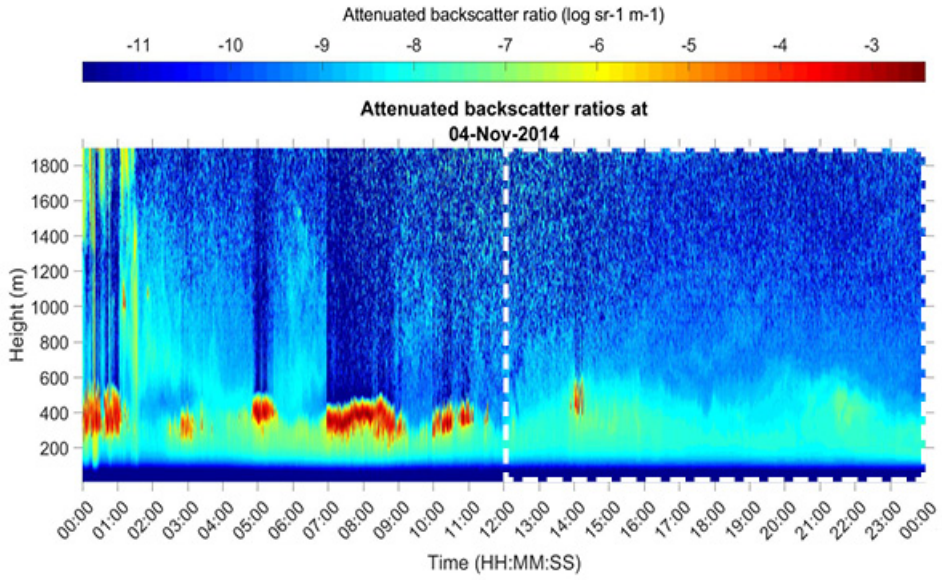

Figure 6.21: ATB height profiles at the 4th of November in 2014.

A general overview of the day is given in Figure 6.21. The time interval for which the RH stays constant (<10% variation) is indicated in the figure with a white rectangle. Signals before 2:00 can't be used to draw any conclusions as the ATB is mostly saturated.

In Figure 6.22, the RH and ATB at 200 meter are compared. ANCs for aerosols with diameters between 9.37-516 nm are also provided to give an indication of the influence of ANC on the ATB. The RH in the selected time interval stays approximately between 85% and 95%. The ATB stays fairly constant. The ATB doesn't seem to be influenced by the ANC as this slightly rises until 18:00, after which it slightly drops again. This behavior is not seen in the ATB plot, however the changes in ANC are very small. There is no AOD data from AERONET available for this day [5].

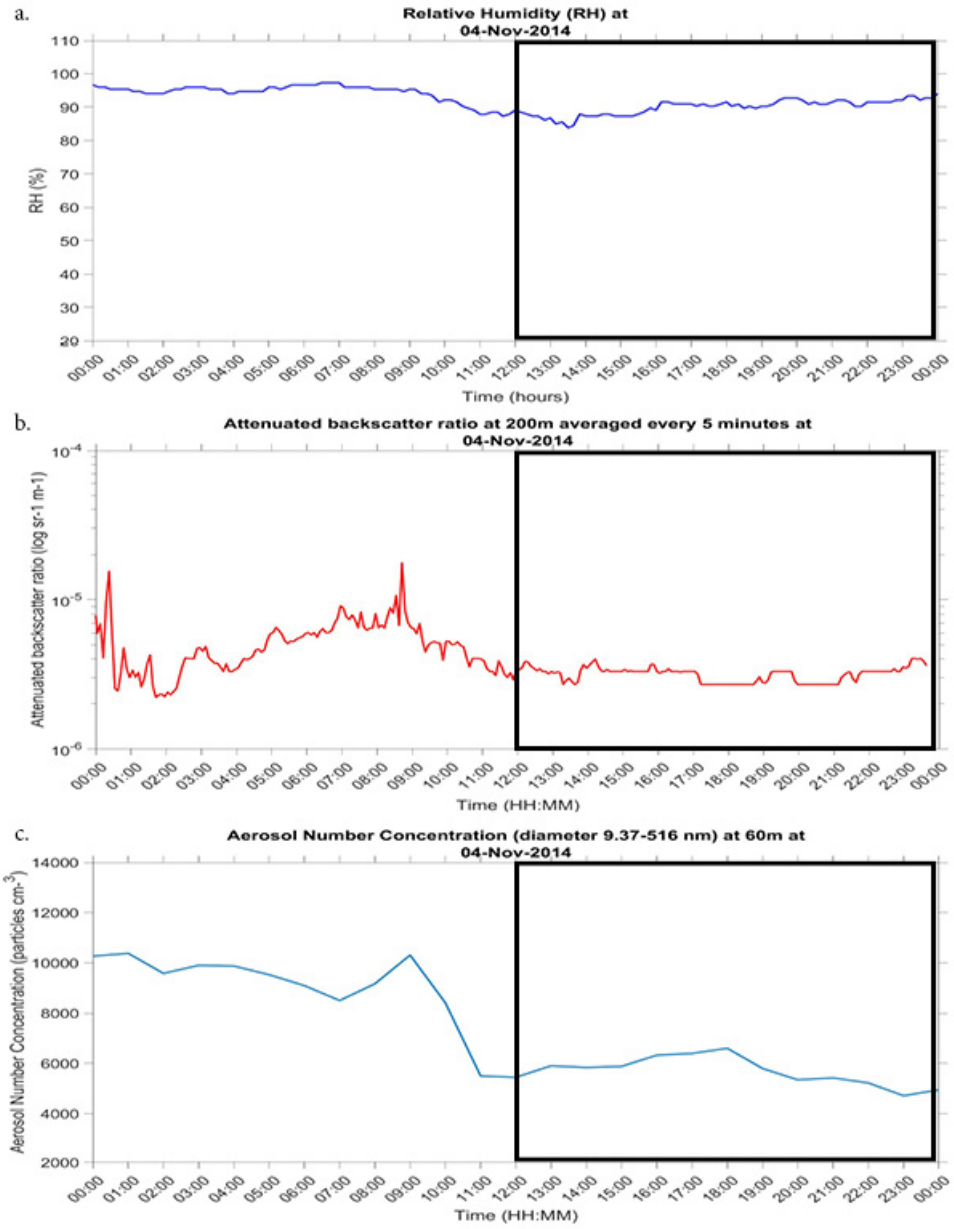

Figure 6.22: RH and ATB at 200 meter and ANC (diameter = 9.37 - 516 nm) at 60 meter at the 4th of November in 2014.

6.2.5. 12th of November

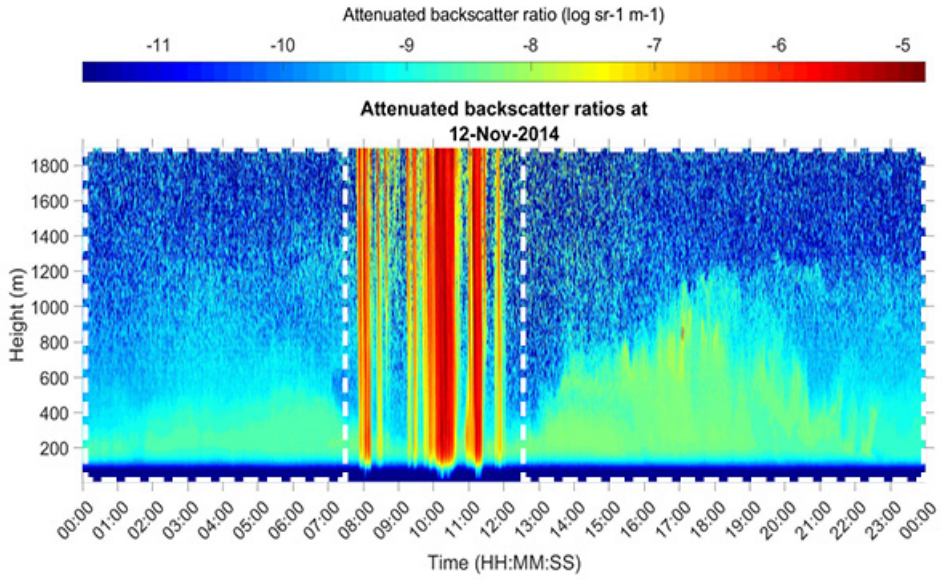

Figure 6.23: ATB height profiles at the 12th of November in 2014.

A general overview of the day is given in Figure 6.23. Almost the whole day was suitable for the analysis, except the 7:30 - 12:30 interval as ATB signals are mostly saturated.

In Figure 6.24, the RH and ATB at 200 meter are compared. ANCs for aerosols with diameters between 9.37-516 nm are also provided to give an indication of the influence of ANC on the ATB. The RH in the selected time interval stays approximately between 80% and 90%. The ATB stays fairly constant. The ATB doesn't seem to be influenced by the ANC as the drops and rises in aerosols aren't shown in drops and rises in ATB. There is no AOD data from AERONET available for this day [5].

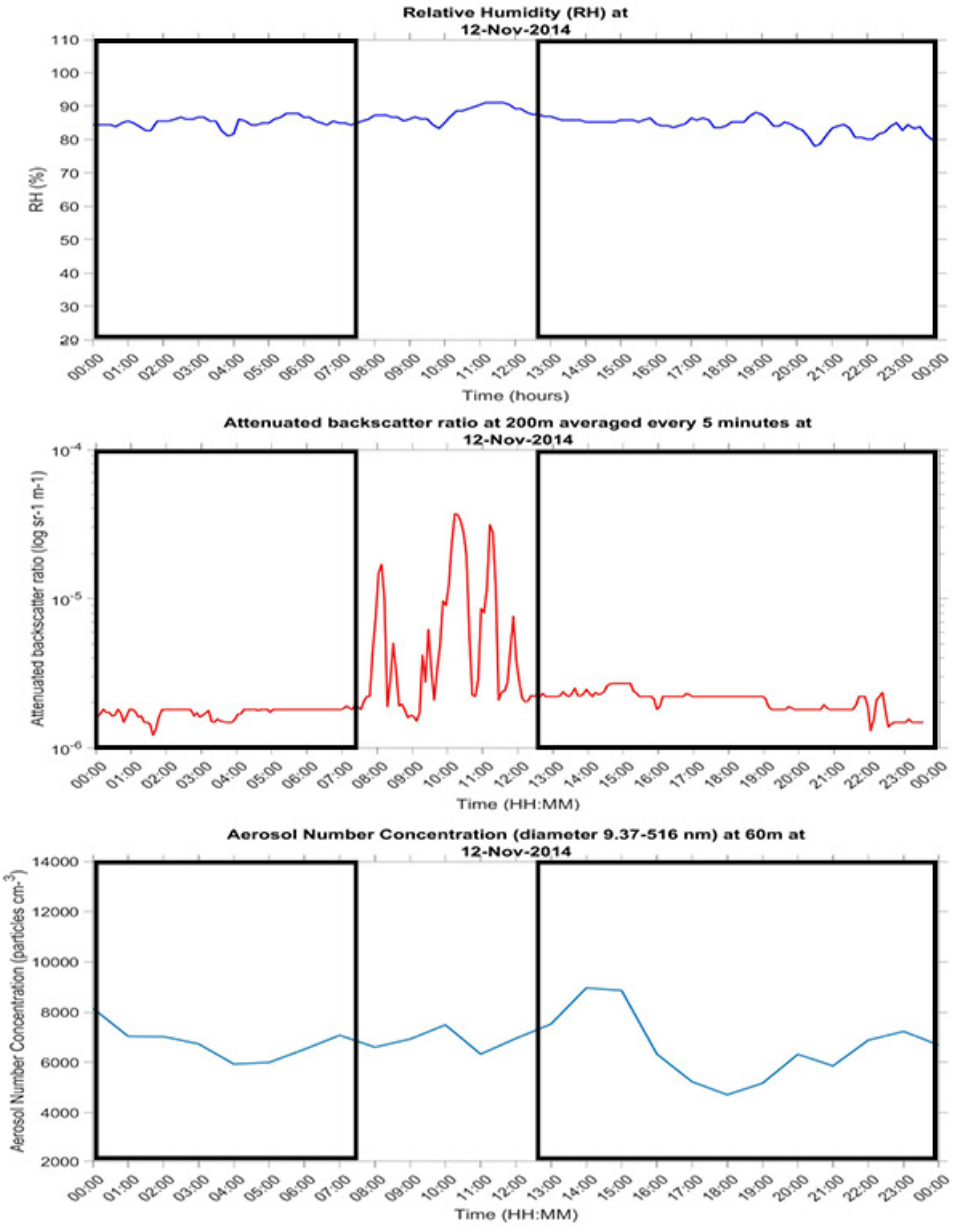

Figure 6.24: RH and ATB at 200 meter and ANC (diameter = 9.37 - 516 nm) at 60 meter at the 12th of November in 2014.

7

Conclusion and Recommendations

By comparing relative humidity (RH) and attenuated backscatter ratio (ATB) data, an attempt is made to better understand the process of aerosol hygroscopic growth. By using a ground based ceilometer, hygrometer and Scanning Mobility Particle Sizer (SMPS) technology during the ACCEPT campaign at Cabauw, a high temporal resolution, continuous measurements and the possibility to compare the data with ancillary information produced on the same location is obtained.
During the three time intervals with a rise or drop in RH >30% that are studied in this paper (being the 15th and 25th of October and 10th of November 2014), a clear correlation is found between RH and ATB values. The asymptotic behavior seems to resemble the Köhler curve (Figure 3.2), when a direct relation between aerosol diameter and ATB is assumed. For the five time intervals with constant RH (<10% variation) that are studied in this paper (namely the 13th, 25th and 30th of October and the 4th and 12th of November 2014), no large changes in ATB signal are observed. This also points towards a clear correlation between RH and ATB values.
As the aerosol number concentration (ANC) could also influence ATB values, ANC values for particles with diameters between 9.37-516 nm are taken into account. Although these small particles are not expected to have a large influence on the ATB, these values are used as indication of the influence ANC could have on ATB. For more data on ANC, aerosol optical depth (AOD) values are take into account as well, consulted from the AERONET (aerosol robotic network) website. Unfortunately, not all days had sufficient AOD data to draw additional conclusions. So far, no definite conclusions can be drawn on the influence of ANC on ATB for these case days. The data that was available however didn't point towards a strong correlation between ANC and ATB for the analyzed time intervals.
The scattering hygroscopic enhancement factor derived for the three time intervals with a rise or drop in RH >30% (being the 15th and 25th of October and 10th of November 2014). These give similar γ values as reported in previous studies [7], namely 0.8081, 0.9342 and 0.3621 for the three respective time intervals. As all used RH values lie between 60% and 100% (after all RH > 100% values are removed), the lowest RH value per day is used as RH_{dry}. The aerosols are not expected to be completely dry at RH values between 60% and 70% but haven't grown too much for an estimation of the scattering hygroscopic enhancement factor.

For further research, more representative ANC data is recommended to better understand the relation between ANC and ATB. Also the use of chemical composition data of the aerosols can give more clarity on the exact correlation between RH and ATB. For the derivation of the scattering hygroscopic enhancement factor, it is advised to use case studies that have a larger range in RH values, for example from 30% to 100%. This way, aerosols that are completely dry can also be taken into account. As a correlation between RH and ATB is now only demonstrated in three examples, it is also recommended to study a longer period of time to collect more suitable data for further analysis.

Bibliography

[1] KNMI - Determination of the mixing layer height from ceilometer backscatter profiles. URL https://www.knmi.nl/kennis-en-datacentrum/achtergrond/determination-of-the-mixing-layer-height-from-ceilometer-backscatter-profiles.

[2] M. O. Andreae and D. Rosenfeld. Aerosol-cloud-precipitation interactions. Part 1. The nature and sources of cloud-active aerosols. *Earth-Science Reviews*, 89(1-2):13–41, 2008. ISSN 00128252. doi: 10.1016/j.earscirev.2008.03.001.

[3] Fred C Bosveld. Cabauw In-situ Observational Program 2000 – Now : Instruments , Calibrations and Set-up. 2017. URL http://projects.knmi.nl/cabauw/insitu/observations/documentation/Cabauw{_}TR/Cabauw{_}TR.pdf.

[4] O. Boucher, D. Randall, Paulo Artaxo, C. Bretherton, G. Feingold, P. Forster, V-M V.-M. Kerminen, Y. Kondo, H. Liao, U. Lohmann, P. Rasch, S. K. Satheesh, S. Sherwood, B. Stevens, X Y Zhang, and X. Y Zhan. Clouds and Aerosols. *Climate Change 2013: The Physical Science Basis. Contribution of Working Group I to the Fifth Assessment Report of the Intergovernmental Panel on Climate Change*, pages 571–657, 2013. ISSN 9781107415324. doi: 10.1017/CBO9781107415324.016.

[5] David M. Giles. AERONET Aerosols. URL https://aeronet.gsfc.nasa.gov/new{_}web/aerosols.html.

[6] A. J. Fernández, A. Apituley, I. Veselovskii, A. Suvorina, J. Henzing, M. Pujadas, and B. Artinano. Study of aerosol hygroscopic events over the Cabauw experimental site for atmospheric research (CESAR) using the multi-wavelength Raman lidar Caeli. *Atmospheric Environment*, 120:484–498, 2015. ISSN 18732844. doi: 10.1016/j.atmosenv.2015.08.079.

[7] M. J. Granados-Muñoz, F. Navas-Guzmán, J. A. Bravo-Aranda, J. L. Guerrero-Rascado, H. Lyamani, A. Valenzuela, G. Titos, J. Fernández-Gálvez, and L. Alados-Arboledas. Hygroscopic growth of atmospheric aerosol particles based on active remote sensing and radiosounding measurements: Selected cases in southeastern Spain. *Atmospheric Measurement Techniques*, 8(2):705–718, 2015. ISSN 18678548. doi: 10.5194/amt-8-705-2015.

[8] Martial Haeffelin. TNA-HYGRO-ACTRIS-4.

[9] Martial Haeffelin, Quentin Laffineur, Juan Antonio Bravo-Aranda, Marc Antoine Drouin, Juan Andrés Casquero-Vera, Jean Charles Dupont, and Hugo De Backer. Radiation fog formation alerts using attenuated backscatter power from automatic lidars and ceilometers. *Atmospheric Measurement Techniques*, 9(11):5347–5365, 2016. ISSN 18678548. doi: 10.5194/amt-9-5347-2016.

[10] T. Hamburger, G. McMeeking, A. Minikin, A. Petzold, H. Coe, and R. Krejci. Airborne observations of aerosol microphysical properties and particle ageing processes in the troposphere above Europe. *Atmospheric Chemistry and Physics*, 12(23):11533–11554, 2012. ISSN 16807316. doi: 10.5194/acp-12-11533-2012.

[11] Robert a. Kotchenruther, Peter V. Hobbs, and Dean a. Hegg. Humidification factors for atmospheric aerosols off the mid-Atlantic coast of the United States. *Journal of Geophysical Research*, 104(D2):2239–2251, 1999. ISSN 0148-0227. doi: 10.1029/98JD01751.

[12] Ying Li and Chang-Yu Wu. Atmospheric Aerosol. URL https://aerosol.ees.ufl.edu/atmos{_}aerosol/section01.html.

[13] U Lohmann and J Feichter. Global indirect aerosol effects: a review. *Atmospheric Chemistry and Physics*, 5:715–737, 2005. URL www.atmos-chem-phys.org/acp/5/715/.

[14] David C Lowe and New Zealand. Changes in Atmospheric Constituents and in Radiative Forcing (IPCC 2007). *Change*, 30(22):129–234, 2007. ISSN 1930529X. doi: 10.1103/PhysRevB.77.220407. URL http://en.scientificcommons.org/23467316.

[15] Ray McGrath, Tido Semmler, Conor Sweeney, and Shiyu Wang. Impact of balloon drift errors in radiosonde data on climate statistics. *Journal of Climate*, 19(14):3430–3442, 2006. ISSN 08948755. doi: 10.1175/JCLI3804.1.

[16] A. A. Mensah, R. Holzinger, R. Otjes, A. Trimborn, Th F. Mentel, H. Ten Brink, B. Henzing, and A. Kiendler-Scharr. Aerosol chemical composition at Cabauw, the Netherlands as observed in two intensive periods in May 2008 and March 2009. *Atmospheric Chemistry and Physics*, 12(10):4723–4742, 2012. ISSN 16807316. doi: 10.5194/acp-12-4723-2012.

[17] W. T. Morgan, J. D. Allan, K. N. Bower, M. Esselborn, B. Harris, J. S. Henzing, E. J. Highwood, A. Kiendler-Scharr, G. R. McMeeking, A. A. Mensah, M. J. Northway, S. Osborne, P. I. Williams, R. Krejci, and H. Coe. Enhancement of the aerosol direct radiative effect by semi-volatile aerosol components: Airborne measurements in North-Western Europe. *Atmospheric Chemistry and Physics*, 10(17):8151–8171, 2010. ISSN 16807316. doi: 10.5194/acp-10-8151-2010.

[18] Christodoulos Pilinis, Spyros N. Pandis, and John H. Seinfeld. Sensitivity of direct climate forcing by atmospheric aerosols to aerosol size and composition. *Journal of Geophysical Research*, 100(D9):18739, 1995. ISSN 0148-0227. doi: 10.1029/95JD02119. URL http://doi.wiley.com/10.1029/95JD02119.

[19] John H Seinfeld and John Wiley. *ATMOSPHERIC From Air Pollution to Climate Change SECOND EDITION*, volume 51. 2006. ISBN 9780471720171. doi: 10.1016/0016-7037(87)90252-3. URL http://adsabs.harvard.edu/abs/1998acpa.conf...S {\char"00DC\relax}.

[20] Roland Stull. *Practical_Meteorology_1860.Pdf*. 2017. ISBN 9780888652836.

[21] I N Tang and H R Munkelwitz. Water activities, densities, and refractive indices of aqueous sulfates and sodium nitrate droplets of atmospheric importance. 99(94), 1994.

[22] G. Titos, A. Cazorla, P. Zieger, E. Andrews, H. Lyamani, M. J. Granados-Muñoz, F. J. Olmo, and L. Alados-Arboledas. Effect of hygroscopic growth on the aerosol light-scattering coefficient: A review of measurements, techniques and error sources. *Atmospheric Environment*, 141:494–507, 2016. ISSN 18732844. doi: 10.1016/j.atmosenv.2016.07.021. URL http://dx.doi.org/10.1016/j.atmosenv.2016.07.021.

[23] S. Twomey. The Influence of Polution on the Shortwave Albedo of Clouds. *American Meteorological Society*, 1976. URL http://journals.ametsoc.org/doi/pdf/10.1175/1520-0469{%}281977{%}29034{%}3C1149{%}3ATIOPOT{%}3E2.0.CO{%}3B2.

[24] Vaisala Oyj. Vaisala LD-40 Ceilometer Cloud Height Measurement up to High Cirrus. URL http://www.iag.co.at/uploads/tx{_}iagproducts/pdf{_}handbuch/LD-40.de.pdf.

[25] Adam Voiland. Aerosols: Tiny Particles, Big Impact : Feature Articles, nov 2010. URL https://earthobservatory.nasa.gov/Features/Aerosols/page1.php.

[26] E. P. Weijers, M. Schaap, L. Nguyen, J. Matthijsen, H. A.C. Denier Van Der Gon, H. M. Ten Brink, and R. Hoogerbrugge. Anthropogenic and natural constituents in particulate matter in the Netherlands. *Atmospheric Chemistry and Physics*, 11(5):2281–2294, 2011. ISSN 16807316. doi: 10.5194/acp-11-2281-2011.

[27] P. Zieger, E. Weingartner, J. Henzing, M. Moerman, G. De Leeuw, J. Mikkilä, M. Ehn, T. Petäjä, K. Clémer, M. Van Roozendael, S. Yilmaz, U. Frieß, H. Irie, T. Wagner, R. Shaiganfar, S. Beirle, A. Apituley, K. Wilson, and U. Baltensperger. Comparison of ambient aerosol extinction coefficients obtained from in-situ, MAX-DOAS and LIDAR measurements at Cabauw. *Atmospheric Chemistry and Physics*, 11(6):2603–2624, 2011. ISSN 16807316. doi: 10.5194/acp-11-2603-2011.

[28] P. Zieger, R. Fierz-Schmidhauser, E. Weingartner, and U. Baltensperger. Effects of relative humidity on aerosol light scattering: Results from different European sites. *Atmospheric Chemistry and Physics*, 13(21):10609–10631, 2013. ISSN 16807316. doi: 10.5194/acp-13-10609-2013.

A

Supervisor Meetings

A.1. Overview of meetings with supervisors

14-09-2017 & 27-10-2017	Exploratory meetings with Herman Russchenberg
14-11-2017 & 16-11-2017	ACTRIS
20-11-2017	Kick-off meeting with Herman Russchenberg, Dimitra Mamali and Stephanie Rusli
01-12-2017	Work plan meeting with Herman Russchenberg and Dimitra Mamali
20-12-2017	Midterm meeting with Dimitra Mamali

A.2. Exploratory meetings with Herman Russchenberg

Before this meeting, I was not sure yet whether I wanted to do my bachelor thesis at Geoscience & Remote Sensing. Herman's thesis proposal was to study the influence of aerosols on cloud properties. We mainly discussed the basics of aerosol-cloud interaction as I had no prior knowledge on this subject. With a better view on the overall topic I left the meeting. A few weeks later I decided to go with the topic and requested some general reading material on aerosol-cloud interaction. Herman sent me two recent papers by Karolina Sarna and himself on ground-based remote sensing for monitoring aerosol–cloud interactions.
The second exploratory meeting, Herman and I discussed the papers I had read and some thoughts more specific research topics. He wasn't available during the first week of quarter 2 as the ACTRIS conference was in Delft that week. Herman invited me to join two mornings of ACTRIS to gain inspiration on a research topic.

A.3. ACTRIS

The first morning of ACTRIS I joined was about Aerosol Remote Sensing. I met my second supervisor here, Dimitra Mamali. She provided me with some extra general reading material on aerosol cloud interaction.
The second morning was on Clouds, Aerosol and Trace gases Remote Sensing. Herman introduced me to Stephanie Rusli, she would be able to help me with my thesis as well. During this science session, Martial Haeffelin presented his research on investigating aerosol hygroscopic enhancement factors by combining automatic remote sensing instrumentation and chemical characterization, which would be of great inspiration for my thesis topic.

A.4. Kick-off meeting with Herman Russchenberg, Dimitra Mamali and Stephanie Rusli

During the kick-off meeting, we discussed Martials ACTRIS presentation and the topic of relating relative humidity with the lidar backscatter ratio. Dimitra and Stephanie would help me with acquiring and processing data. CESAR data could be used, additional information could be found in the data from the ACCEPT campaign in 2014. We agreed that I would send Herman a planning proposal in two days to define the subtopics I would be looking into and to fit them in the eight weeks at hand.

A.5. Work plan meeting with Herman Russchenberg and Dimitra Mamali

During the work plan meeting, we discussed the planning I made and the upcoming midterm presentation. Herman and Dimitra posed some difficult questions where I should have a sharp answer to during the presentation. As I started one week later than other students, we decided I would mostly present the importance of my research and the steps I was going to take. We also discussed my progress so far, as I analyzed the relative humidity during the 42 days of the ACCEPT campaign and selected 8 days with a big (>30%) drop or rise within one day. Herman warned me that I shouldn't only look at those 8 days as I would steer to much towards an answer, I should keep all options open and take all 42 days into account.

A.6. Midterm meeting with Dimitra Mamali

With both supervisors not being in the Netherlands during the midterm meeting week, I had a skype meeting with only Dimitra to discuss my progress. After selecting the Relative Humidity data with a big drop or rise, I look at the attenuated backscatter ratio of these 8 days. We planned to use CT75 ceilometer data but it turned out to be shut down in 2013 due to a strongly decreased sensitivity. Henk Klein Baltink, KNMI scientific staff working at CESAR provided me with LD40 ceilometer data for 2014. The data was a bit blocky for low backscatter values, so I averaged the backscatter in intervals of 5 and 10 minutes. During the midterm meeting we compared the relative humidity plots and the (averaged) attenuated backscatter ratio plots to see whether there was a relation. We decided that I should zoom in more on the actual hours during the day where the RH drop or rise is to make a better comparison.